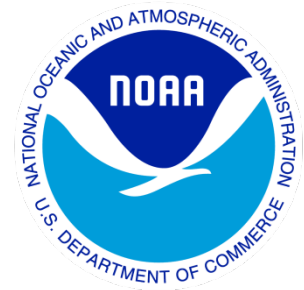# Climate Data Record (CDR) Program

Climate Algorithm Theoretical Basis Document (C-ATBD)

AVHRR Cloud Properties – PATMOS-x

ABI Cloud Height Algorithm (ACHA)

REVISION HISTORY

Rev.	Author	DSR No.	Description	Date
1	Andrew Heidinger, NOAA	DSR-653	Original document – revised for NCDC CDR program formatting by Steve Wanzong	04/04/2014

TABLE of CONTENTS

LIST of FIGURES

LIST of TABLES

A controlled copy of this document is maintained in the CDR Program Library.

Approved for public release. Distribution is unlimited.

7

A controlled copy of this document is maintained in the CDR Program Library.

Approved for public release. Distribution is unlimited.

9

1.   Introduction

1.1   Purpose

The purpose of this document is to describe the GOES-R ABI Cloud Height Algorithm (ACHA) submitted to the National Climatic Data Center (NCDC) by the PATMOS-x development team that will be used to create the cloud-top height, cloud-top temperature, and cloud-top pressure Climate Data Record (CDR), using Advanced Very High Resolution Radiometer (AVHRR) measurements from the NOAA and EumetSat polar orbiting satellites series. The actual algorithm is defined by the computer program (code) that accompanies this document, and thus the intent here is to provide a guide to understanding that algorithm, from both a scientific perspective and in order to assist a software engineer or end-user performing an evaluation of the code. This document will describe the required inputs, the theoretical foundation of the algorithms, the sources and magnitudes of the errors involved, practical considerations for implementation, and the assumptions and limitations associated with the product, as well as provide a high level description of the physical basis for estimating the height of the tops of clouds observed by the imager. Unless otherwise stated, the determination of cloud-top height always implies the simultaneous determination of temperature and pressure. The cloud-top height is made available to all subsequent algorithms that require knowledge of the vertical extent of the clouds.

1.2   Definitions

Following is a summary of the symbols used to define the algorithm.

Spectral and directional parameters:

μ = *wavelength (μm)*   *(1.1)*

K = *temperature in degrees Kelvin*   *(1.2)*

λ = *wavelength*   *(1.3)*

σ^2_{instr} = *instrument noise and calibration uncertainties*   *(1.4)*

σ^2_{clear} = *clear sky radiative transfer uncertainties*   *(1.5)*

σ^2_{hetero} = *forward model uncertainty in regions of large spatial heterogeneity* *(1.6)*

km = kilometers   *(1.7)*

hPa = hectopascals   *(1.8)*

Atmospheric parameters:

β = *cloud microphysical index.*   *(2.1)*

R_{obs} = *observed top-of-atmosphere radiance*   *(2.2)*

T_c = cloud temperature $\hfill$ (2.3)

$B()$ = Planck Function $\hfill$ (2.4)

$\varepsilon_{tropo}(11\mu m)$ = top of troposphere emissivity at 11 μm $\hfill$ (2.5)

R_{clr} = clear sky radiance $\hfill$ (2.6)

R_{ac} = above cloud emission $\hfill$ (2.7)

tac = above cloud transmission $\hfill$ (2.8)

e_c = cloud emissivity $\hfill$ (2.9)

ω = single scattering albedo $\hfill$ (2.10)

g = asymmetry parameter $\hfill$ (2.11)

σ_{ext} = extinction coefficient $\hfill$ (2.12)

P_c = cloud top pressure $\hfill$ (2.13)

Z_c = cloud top height $\hfill$ (2.14)

Mathematical representations:

Φ = optimal estimation cost function $\hfill$ (3.1)

$\mathbf{x}$ = vector of retrieved parameters $\hfill$ (3.2)

$\mathbf{x_a}$ = vector of a priori values of x $\hfill$ (3.3)

$\mathbf{y}$ = vector of observations $\hfill$ (3.4)

$\mathbf{f}$ = forward model estimate of $\mathbf{y}$ under the assumptions of $\mathbf{x}$ $\hfill$ (3.5)

$\mathbf{S_a}$ = error covariance matrix corresponding to $\mathbf{x_a}$ $\hfill$ (3.6)

$\mathbf{S_y}$ = error covariance matrix for the forward model and measurements $\hfill$ (3.7)

$\mathbf{K}$ = Jacobian matrix $\hfill$ (3.8)

$\mathbf{S_x}$ = covariance error matrix of $\mathbf{x}$ $\hfill$ (3.9)

1.3   Referencing this Document

This document should be referenced as follows:

AVHRR Cloud Properties – PATMOS-x (ACHA) - Climate Algorithm Theoretical Basis Document, NOAA Climate Data Record Program CDRP-ATBD-0522 by CDRP Document Manager> Rev. 1 (2014). Available at http://www.ncdc.noaa.gov/cdr/operationalcdrs.html

1.4   Document Maintenance

The production software package is maintained at NCDC. Any update to the ACHA algorithm that would affect files hosted by the CDR program would initiate a revision and redelivery of the ACHA C-ATBD document.

2. Observing Systems Overview

2.1 Products Generated

The ACHA is responsible for an estimation of the vertical extent for all cloudy satellite imager pixels. In terms of the F&PS, it is responsible directly for the Cloud-Top Pressure, Height and Temperature products. The ACHA results are currently used in the daytime and nighttime cloud optical and microphysical algorithms.

In addition to the cloud height metrics (pressure/temperature/height), the ACHA also provides an estimate of the 11 μm cloud emissivity and a microphysical parameter, β, derived from multiple emissivities that are related to particle size. These products, as described later, are generated automatically by the ACHA and are useful for evaluating the ACHA's performance. The requirements for the ACHA from the F&PS version 2.2 are stated below in Table 1, with height, pressure, temperature, layer from top to bottom for each geographic coverage.

Table 1: Requirements from F&PS version 2.2 for ACHA

Geographic coverage	Vertical Res	Horizontal Res	Measurement Range	Measurement Accuracy	Vendor allocated ground latency	Product measurement precision
CONUS	N/A	2 km	0-20km 100-1000 mbar 180-300K Low, Mid, High	0.5 km 50 mbar 3.0 K 80% POD	266 sec 536 sec N/A 806 sec	1.5 km 150 mbar 5K N/A
MESO	N/A	2 km	0-20km 100-1000 mbar 180-300K Low, Mid, High	0.5 km 50 mbar 3.0 K 80% POD	266 sec N/A 266 sec 266 sec	1.5 km 150 mbar 5K N/A
FD	N/A	2 km	0-20km 100-1000 mbar 180-300K	0.5 km 50 mbar 3.0 K	806 sec 806 sec 806 sec	1.5 km 150 mbar 5K

			Low, Mid, High	80% POD	806 sec	N/A

Furthermore, the GOES-R Series Ground Segment (GS) Project Functional and Performance Specification (F&PS) qualifies these requirements for cloudy regions with emissivities greater than 0.8.

2.2   Instrument Characteristics

The ACHA will operate on each pixel determined to be cloudy or probably cloud by the naive Bayesian Cloud Mask (CM). Table 2 summarizes the current channels that may be used by the ACHA.

Table 2: Available wavelengths used in ACHA

Wavelength (µm)
7.0
8.5
11.2
12.3
13.3

In general, the ACHA relies on the infrared observations to avoid discontinuities associated with the transition from day to night. ACHA performance is sensitive to imagery artifacts or instrument noise.   Most important is our ability to accurately model the clear-sky values of the infrared absorption channels. The ability to perform the physical retrievals outlined in this document requires an accurate forward model, accurate ancillary data and well-characterized spectral response functions.

The ACHA is now a more generic representation of the cloud height algorithm. It works on most passive satellite imagers. The current list of supported geostationary satellites includes the GOES series, MTSAT-1R/2, COMS, and SEVIRI. The same algorithm also works on several polar satellites, including, AVHRR, MODIS, and VIIRS. The ACHA uses only infrared observations in order to provide products that are consistent for day, night and terminator conditions. The ACHA uses an analytical model of infrared radiative transfer imbedded into an optimal estimation retrieval methodology. Cloud-top pressure and cloud-top height are derived from the cloud-top temperature product and the atmospheric temperature profile provided by Numerical Weather Prediction (NWP) data.

The ACHA uses the spectral information provided by the satellite imager to derive cloud-top height information simultaneously with cloud microphysical information. Table 3 lists the currently available ACHA "modes" and respective channel combinations. This information allows the ACHA to avoid making assumptions on cloud microphysics in the retrieval of cloud height. As a consequence, ACHA also generates the intermediate products of 11 μm cloud emissivity and an 11/12, or 11/13.3, or 11/8.5, or 11/7.0 μm microphysical index.

Table 3: List of available ACHA modes with associated channels

ACHA Mode	Channel Combination
0	11.2 μm
1	11.2, 12.3 μm
2	11.2, 13.3 μm
3	11.2, 12.3, 13.3 μm
4	8.5, 11.2, 12.3 μm
5	7.0, 11.2, 12.3 μm
6	7.0, 11.2, 13.3 μm
7	7.0, 11.2 μm

3.   Algorithm Description

3.1   Algorithm Overview

The ACHA serves a critical role in the PATMOS-x processing system. It provides a fundamental cloud property but also provides information needed by other cloud and non-cloud algorithms. As such, latency was a large concern in developing the ACHA. The current version of the ACHA algorithm draws on the following heritage algorithms:

- The CLAVR-x split-window cloud height from NESDIS, and

- The MODIS CO_2 cloud height algorithm developed by the UW/CIMSS.

The ACHA derives the following cloud products listed in the F&PS:

- Cloud-top temperature,

- Cloud-top pressure, and

- Cloud-top height.

All of these products are derived at the pixel level for all cloudy pixels.

In addition, the ACHA derives the following products that are not included in F&PS:

- Quality flags,

- Cloud 11 µm emissivity, and

- Cloud microphysical index (β).

Appendix B describes the full set of outputs from the ACHA algorithm.

3.2   Processing Outline

The processing outline of the ACHA is summarized in Figure 1. The current ACHA is implemented with the NOAA/NESDIS/STAR PATMOS-x processing framework. PATMOS-x routines are used to provide all of the observations and ancillary data. The ACHA is designed to run on segments of data where a segment is comprised of multiple scan lines.

Figure 1: High-level flowchart of the ACHA illustrating the main processing sections.

3.3   Algorithm Input

3.3.1   Primary Sensor Data

The list below contains the primary sensor data used by the ACHA. By primary sensor data, we mean information that is derived solely from the satellite imager observations and geolocation information. See Table 3 for channel information for each ACHA mode.

- Calibrated radiances for the 11 μm channel

- Calibrated brightness temperatures for the channels in the selected ACHA mode

- Cosine of sensor viewing zenith angle

- Satellite zenith angle

- Space mask

- Bad pixel mask for the channels in the selected ACHA mode

3.3.2   Ancillary Data

The following lists the ancillary data required to run the ACHA. A more detailed description is provided in the AIADD. By ancillary data, we mean data that require information not included in the satellite imager observations or geolocation data.

- Surface elevation

- Surface type

- NWP level associated with the surface

- NWP level associated with the tropopause

- NWP tropopause temperature

- Profiles of height, pressure and temperature from the NWP

- Inversion level profile from NWP

- Surface temperature and pressure from NWP

- Viewing Zenith Angle bin

- NWP Line and element indices

- Clear-sky transmission, and radiance profiles for the channels in the ACHA selected mode from the RTM

- Blackbody radiance profiles for the channels in the ACHA selected mode from the RTM

- Clear-sky estimates of the radiances for the channels in the ACHA selected mode from the RTM

3.3.3   Derived Data

The following lists and briefly describes the data that are required by the ACHA that is provided by other algorithms.

- **Cloud Mask**

  A cloud mask is required to determine which pixels are cloudy and which are not, which in turn determines which pixels are processed. The naïve Bayesian Cloud Mask (CM) algorithm provides this data to the ACHA. Details on the CM are provided in Heidinger (2012).

- **Cloud Type/Phase**

  A cloud type and phase are required to determine which *a priori* information for the forward model are used. It is assumed that both the cloud type and phase are inputs to the ACHA algorithm. The Cloud Type/Phase Algorithm provides these products. Information on the Cloud Type/Phase is provided in the ABI Type/Phase ATBD.

- **Local Radiative Centers**

  Given a derived 11μm top of troposphere emissivity, $\varepsilon_{tropo}(11\mu m)$, the local radiative center (LRC) is defined as the pixel location, in the direction of the gradient vector, upon which the gradient reverses or when an emissivity value ($\varepsilon_{tropo}(11\mu m)$) greater than or equal to 0.75 is found, whichever occurs first. The gradient filter routine is required as an input to the ACHA. The method to compute the gradient function is described in Pavolonis (2009) and in the AIADD. The required inputs to the gradient filter are:

  o $\varepsilon_{tropo}(11\mu m)$,

  o The line and element size of the segment being processed,

  o A binary mask for the segment of pixels that have non-missing $\varepsilon_{tropo}(11\mu m)$ for the segment,

  o The minimum and maximum valid emissivity values (0.0 and 1.0 respectively), and

  o The maximum $\varepsilon_{tropo}(11\mu m)$ value to be considered (0.75).

  The outputs from the gradient filter are the line and element of the LRC. A further description of how the LRC is calculated can be found in the AIADD.

- **Derived 11μm top of troposphere emissivity**

  The ACHA requires knowledge of the 11μm emissivity of a cloud assuming that its top coincides with the tropopause. This calculation is done by using the measured 11μm radiance, clear sky 11μm radiance from the RTM, space mask, latitude/longitude cell index from the NWP, tropopause index from the NWP, viewing zenith angle bin index, and 11 ☐m blackbody radiance.

- **Standard deviation of the 11 μm brightness temperature over a 3x3 pixel array.**

- **Standard deviation of the 11 μm – 2nd channel of the selected ACHA mode brightness temperature difference over a 3x3 pixel array.**

- **Standard deviation of the 11 μm – 3rd channel of the selected ACHA mode brightness temperature difference over a 3x3 pixel array.**

3.3.4   Forward Models

The Pressure layer Fast Algorithm for Atmospheric Transmittances (PFAAST) forward model is used in PATMOS-x (Hannon, 1996). It is a fast and accurate transmittance model with calculations made at 101 pressure levels (0.01 – 105 kPa). PFAAST takes into account the satellite zenith angle, absorption by well-mixed gases, water vapor and ozone. For each layer, and channel of the satellite, transmittances are calculated line-by-line for a variety of temperature, humidity's, and ozone.

3.4   Theoretical Description

As described below, the ACHA represents an innovative approach that uses multiple IR channels within an algorithm that provides results that are consistent for all viewing conditions. This approach combines multiple window channel observations with a single absorption channel observations to allow for estimation of cloud height without large assumptions on cloud microphysics for the first time from a geostationary imager. The remainder of this section provides the physical basis for the chosen approach.

The ACHA uses the infrared observations from the satellite imager to extract the desired information on cloud height. Infrared observations are impacted not only by the height of the cloud, but also its emissivity and how the emissivity varies with wavelength (a behavior that is tied to cloud microphysics). In addition, the emissions from the surface and the atmosphere can also be major contributors to the observed signal. Lastly, clouds often exhibit complex vertical structures that violate the assumptions of the single layer plane parallel models (leading to erroneous retrievals). The job of the ACHA is to exploit as much of the information provided by the imager as possible with appropriate, computationally efficient and accurate methods to derive the various cloud height products.

The ACHA represents a merger of current operational cloud height algorithms run by NESDIS on the Polar Orbiting Environmental Satellite (POES) and GOES imagers. The current GOES-NOP cloud height algorithm applies the CO_2 slicing method to the 11 and 13.3 μm observations. This method is referred to as the CO_2/IRW approach. CO_2 slicing was developed to estimate cloud-top pressures using multiple channels typically within the 14 μm CO_2 absorption band. For example, the MODIS MOD06 algorithm (Menzel et al., 2006) employs four CO_2 bands, and the GOES Sounder approach also employs four bands. CO_2 slicing benefits from the microphysical simplicity provided by the spectral uniformity of the cloud emissivity across the 14 μm band. The GOES-NOP method suffers from two weaknesses relative to the MOD06 method. First, the assumption of spectral uniformity of cloud emissivity is not valid when applied to the 11 and 13.3 μm observations. Second, the 13.3 μm channel does not provide sufficient atmospheric opacity to provide the desired sensitivity to cloud height for optically thin high cloud (i.e., cirrus). For optically thick clouds, CO_2 slicing methods rely simply on the 11 μm observation for estimating the cloud height.

In contrast to the CO_2/IRW approach used for GOES-NOP, the method employed operationally for the POES imager (AVHRR) uses a split-window approach based on the 11 and 12 ☐m observations. Unlike the 13.3 ☐m band, the 11 and 12 ☐m bands are in spectral windows and offer little sensitivity to cloud height for optically thin cirrus. As described in Heidinger and Pavolonis (2009), the split-window approach does provide accurate measurements of cloud emissivity and its spectral variation.

Unlike the GOES-NOP imager or the POES Imager, the ABI provides the 13.3 μm CO_2 channels coupled with multiple longwave IR windows (10.4, 11 and 12 μm). The ABI therefore provides an opportunity to combine the sensitivity to cloud height offered by a CO_2 channel with the sensitivity to cloud microphysics offered by window channels and to improve upon the performance of the cloud height products derived from the current operational imagers.

To demonstrate the benefits of the ACHA CO_2/Split-Window algorithm, the sensitivity to cloud pressure offered by the channels used in the ACHA was compared to other channel sets using co-located MODIS and CALIPSO observations. These results where taken from Heidinger et al. (2010). **Figure 2** shows a false color image from AQUA/MODIS for a cirrus scene observed on August 10, 2006 over the Indian Ocean. The red line in **Figure 2** shows the location of the CALIPSO track. This scene is characterized by a predominantly single cirrus cloud of varying optical thickness with thicker regions on the left side of the figure. An image of the 532 nm CALIPSO data for the trajectory shown in **Figure 2** is shown in **Figure 3**.
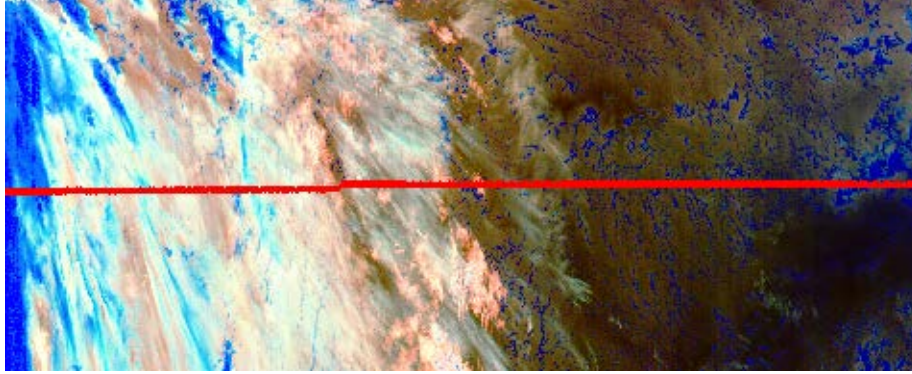
Figure 2: A false color image constructed from 11 – 12 μm BTD (Red), 4 – 11 μm BTD (Green) and 11 μm BT reversed (Blue). Data are taken from AQUA/MODIS and CALIPSO/CALIOP on August 10, 2006 from 20:35 to 20:40 UTC. The red line is the CALIPSO track. In this color combination, cirrus clouds appear white but as the optical thickness increases, the ice clouds appear as light blue/cyan. Low-level water clouds appear as dark blue, and mid-level water clouds tend to have a red/orange color.
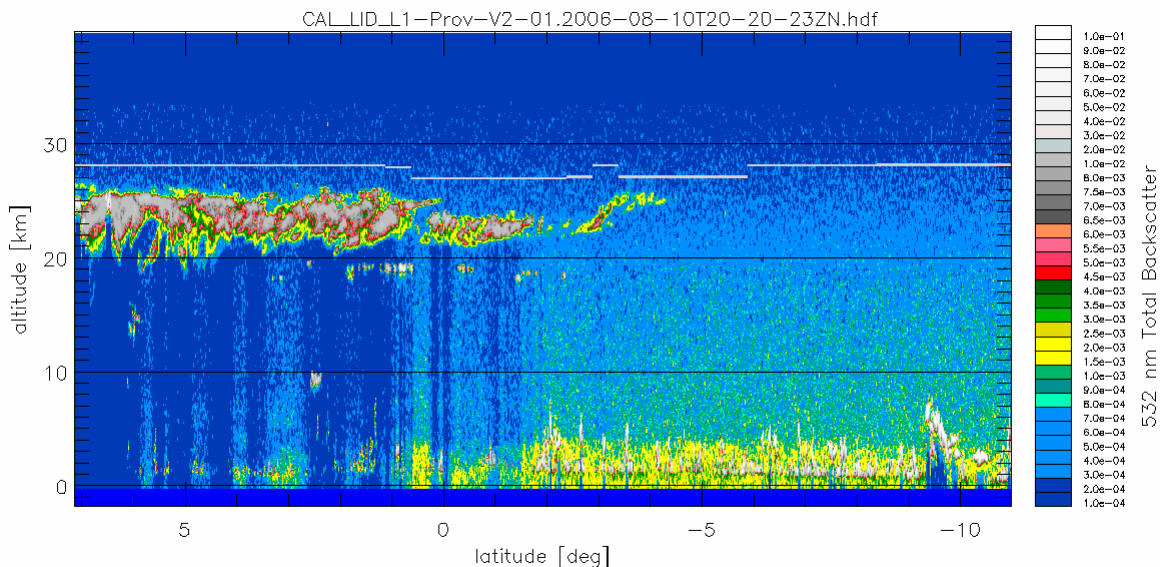
Figure 3: The 532 nm total backscatter from CALIOP along the red line shown in Figure 2. The grey line in the center image is the Tropopause.

In the work of Heidinger et al. (2009), an analysis was applied to the above data to study the impact on the cloud-top pressure solution space offered by various channel combinations commonly used on operational imagers. The term solution space refers to the vertical region in the atmospheric column where a cloud can exist and match the observations of the channels used in the algorithm. As described in Heidinger et al. (2009) this analysis was accomplished specifically by computing the emissivity profiles for each

channel and determining the levels at which the emissivities were all valid and where the spectral variation of the emissivities was consistent with the chosen scattering model. It is important to note that this analysis was not a comparison of algorithms, but a study of the impact of the pixel spectral information on the possible range of solutions.

    Figure 4 shows the resulting computation of the cloud-top pressure solution space spanned by the ACHA CO_2/Split-Window algorithm (channels 11, 12 & 13.3 μm). The grey area represents the region of the atmosphere where the MODIS observations of those channels were matched to within 0.5K. The blue points represent the cloud-top pressures where the cloud matched the MODIS observation most closely. In contrast, **Figure 5** shows the same computation when using the VIIRS cloud-top height algorithm's channel set. As described by Heidinger et al. (2009), the large improvement in the sensitivity to cloud top pressure seen in ACHA versus the VIIRS algorithm is due to the presence of the CO_2 absorption channel. Because VIIRS offers only IR window channels, its ability to estimate the height of cirrus clouds with confidence is limited.
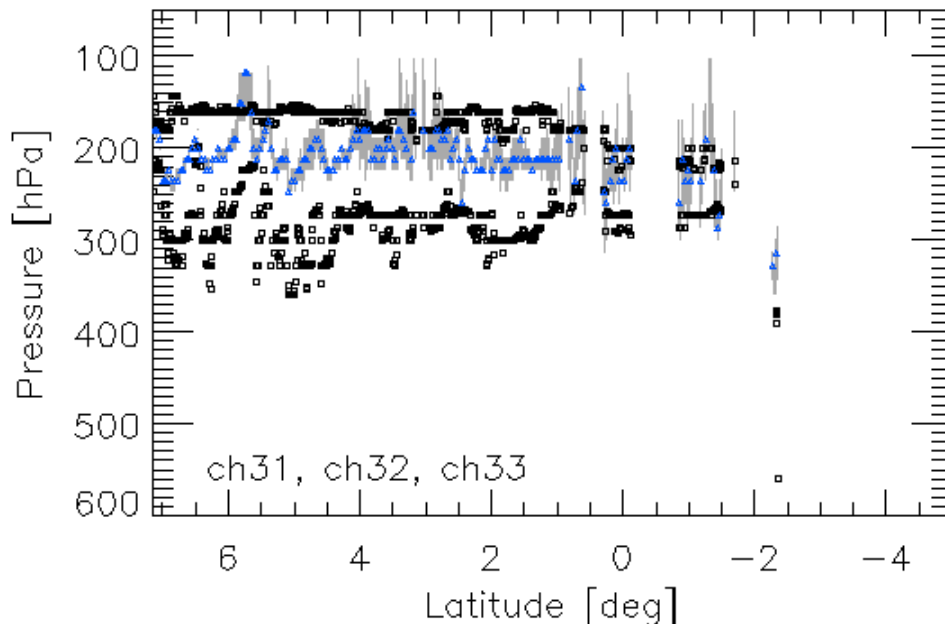
Figure 4: Cloud-top pressure solution space provided by the ACHA channel set for the ice clouds along the CALIPSO track for August 10, 2006 20:35 – 20:40 UTC. The grey lines represent the solution space provided by the selected GOES-R ABI channels. The black symbols provide the CALIOP cloud boundaries for the highest cloud layer. The blue points represent the location of the optimal cloud-top pressure solutions with this channel set. For clarity, only every fifth optimal cloud-top pressure solution is plotted.
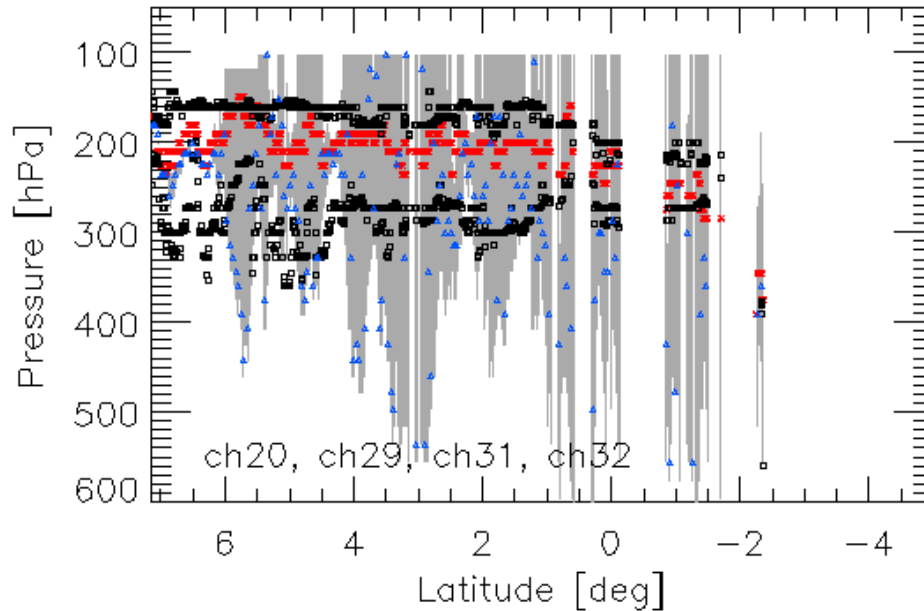
Figure 5: Same as Figure 4 computed for the VIIRS channel set (3.75, 8.5, 11 and 12 μm). Red points show the MODIS (MYD06) results for reference.

3.4.1 Physical and Mathematical Description

3.4.1.1 Radiative Transfer Equation

The radiative transfer equation (1) employed here is given as

$$R_{obs} = e_c R_{ac} + t_{ac} e_c \, B(T_c) + R_{clr}(1 - e_c) \qquad (1)$$

where R_{obs} is the observed top-of-atmosphere radiance, T_c is the cloud temperature, B() represents the Planck Function and R_{clr} is the clear-sky radiance (both measured at the top of the atmosphere). R_{ac} is the above-cloud emission; t_{ac} is the above-cloud transmission along the path from the satellite sensor to the cloud pixel. Finally, the cloud emissivity is represented by e_c. All quantities in Eq. 1 are a function of wavelength, λ, and are computed separately for each channel.

As described later, the 11 μm cloud emissivity is directly retrieved by the ACHA. The cloud emissivities of the channels used in the selected ACHA mode are not retrieved but they are utilized during the retrieval process.

To account for the variation of e_c with each channel, the β parameter is evoked. For any two-channel pair (1,2), the value of β can be constructed using the following relationship:

$$\beta_{1,2} = \ln(1-e_2)/\ln(1-e_1) \tag{2}$$

Using this relationship, the cloud emissivities at, for example using the 12 and 13.3 μm channels, can be derived from the cloud emissivity value at 11 μm as follows:

$$e_c(12\mu m) = 1 - [1 - e_c(11\mu m)]^{\beta(12/11\mu m)} \tag{3}$$

$$e_c(13.3\mu m) = 1 - [1 - e_c(11\mu m)]^{\beta(13.3/11\mu m)} \tag{4}$$

For the remainder of this document, the value of e_c will refer to the cloud emissivity at 11 μm and β will refer to the β(11/12 $\Box$ m) value unless a convenient parameter because it also provides a direct link to cloud microphysics, which is discussed in the next section.

While the above radiative transfer equation is simple in that it assumes no scattering and that the cloud can be treated as a single layer, it does allow for semi-analytic derivations of the observations to the controlling parameters (i.e., cloud temperature). This behavior is critical because it allows for an efficient retrieval without the need for large lookup tables.

3.4.1.2 Cloud Microphysical Assumptions

One of the strengths of the ACHA is that it allows cloud microphysics to vary during the retrieval process, which should improve the cloud height estimates (Heidinger et al., 2009). Cloud microphysics is included in the retrieval through the spectral variation of the β parameters. The variation of β between different channel pairs is a function of particle size and ice crystal habit. For example, Parol et al. (1991) showed that β can be related to the scattering properties using the following relationship where ω is the single scattering albedo, g is the asymmetry parameter and σ_{ext} is the extinction coefficient:

$$\beta_{2,1} = \frac{[1.0 - \omega(\lambda_1)g(\lambda_1)]\sigma_{ext}(\lambda_1)}{[1.0 - \omega(\lambda_2)g(\lambda_2)]\sigma_{ext}(\lambda_2)} \tag{5}$$

This relationship between β and the scattering properties will allow the ACHA to estimate cloud particle size from the retrieved β values.

While the scattering properties for water clouds are well modeled by Mie theory, the scattering properties of ice clouds are less certain. To define a relationship between the β values for ice clouds, assumptions have to be made about the ice crystals. In the ACHA, we use the ice scattering models provided by Professor Ping Yang at Texas A&M University (Yang et al., 2005). In this database, ice models are separated by habits. To pick a habit, β values were computed using MODIS observations collocated with CALIPSO. We then compared how the observed β values corresponded with those computed from the scattering. The results indicated that aggregates modeled the observed data the best. The image below (**Figure 6**) shows this analysis, which was generated for August 2006. For

A controlled copy of this document is maintained in the CDR Program Library.

Approved for public release. Distribution is unlimited.

25

water clouds, standard Mie theory computed scattering properties are used to predict the β values and their relationship with each other.
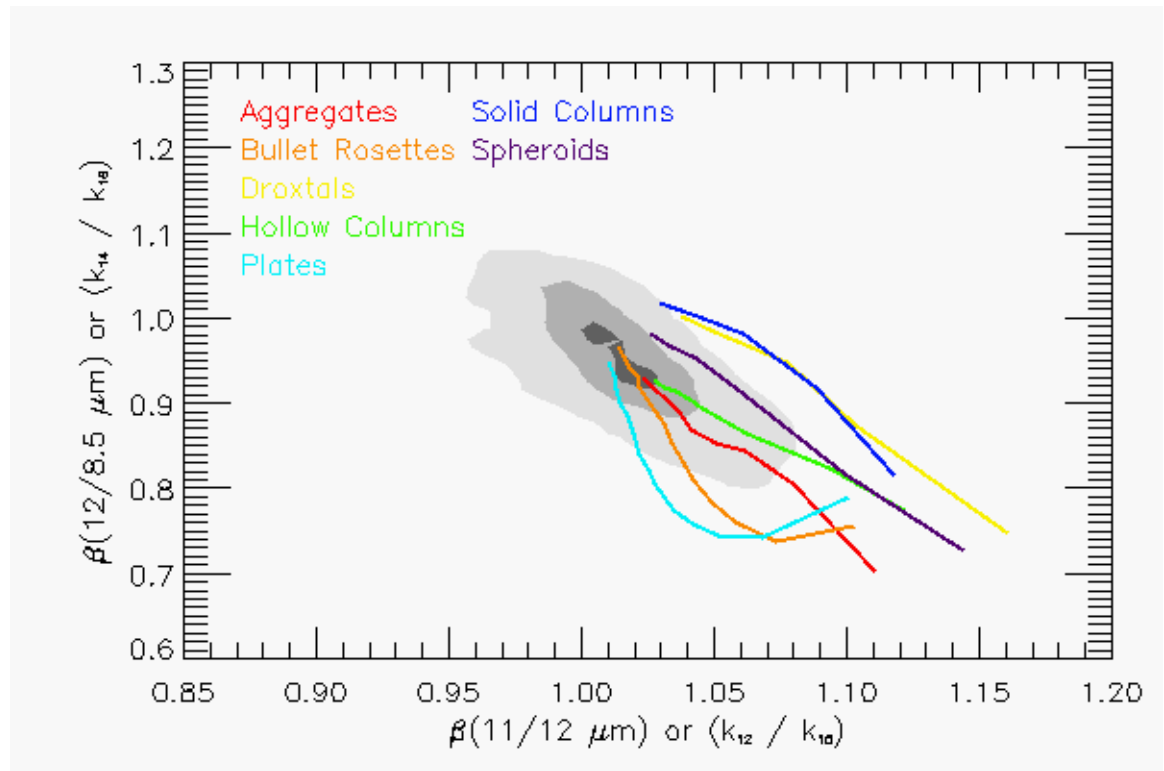
Figure 6: Comparison of the variation of β values for 11 and 12 μm against those for 12 and 8.5 μm. The cloud of points represents those computed using CALIPSO observations collocated with MODIS. The lines represent predictions based on the Yang et. al scattering database.

        Once the habit has been determined, the needed β relationships can be computed. **Figure 7** shows the computed variation of the 11 and 12 μm β with the 11 and 13.3 μm β and **Figure 8** shows the variation of the 11 and 12 μm β with particle size. These curves and the regressions shown in **Figure 7** and **Figure 8** are used directly in the optimal estimation approach described in the next section.
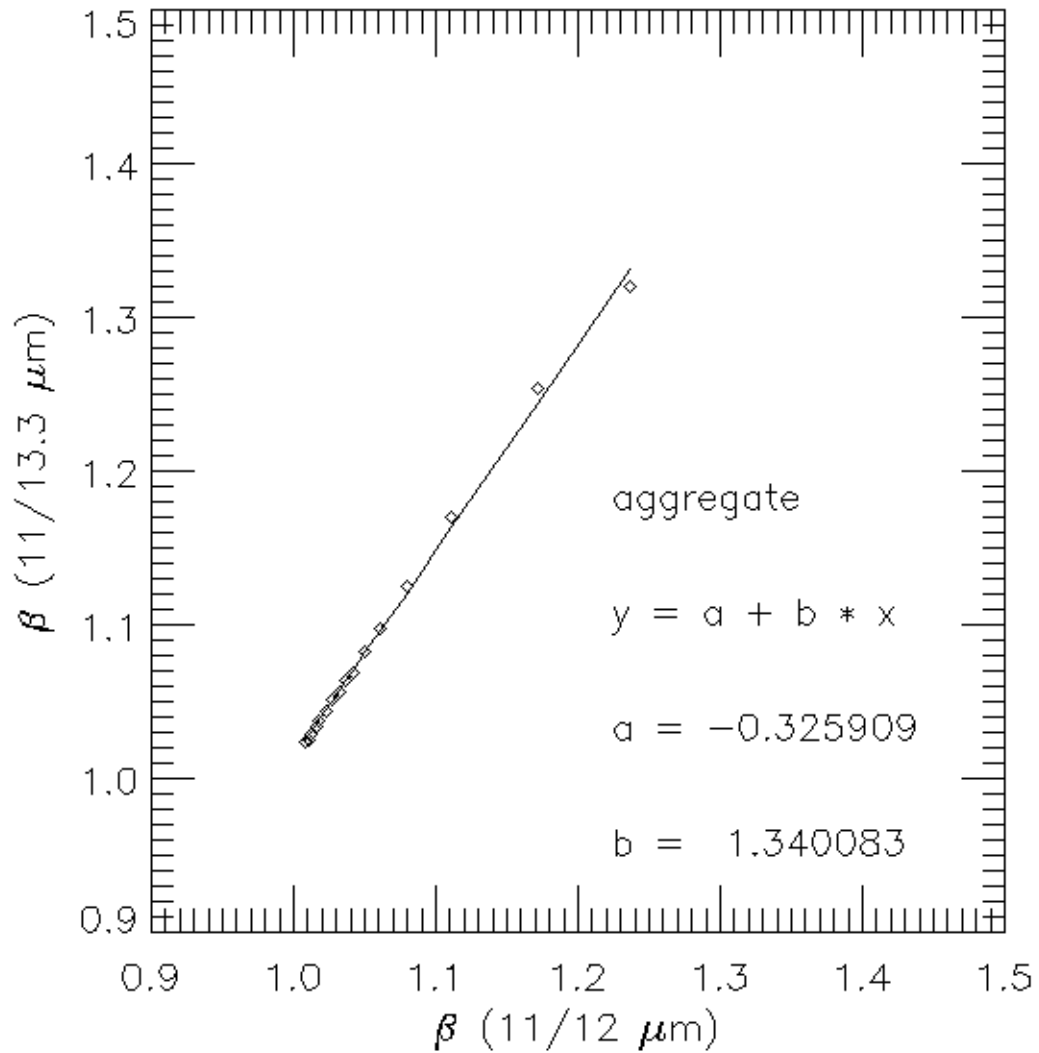
Figure 7: Computed variation and linear-fit of the 11 and 13.3 μm β values to those computed using 11 and 12 μm. β is a fundamental measure of the spectral variation of cloud emissivity, and this curve is used in the forward model in the retrieval. The data shown are for ice crystals with an aggregate habit. For water clouds, Mie theory predicts a = -0.217 and b = 1.250.
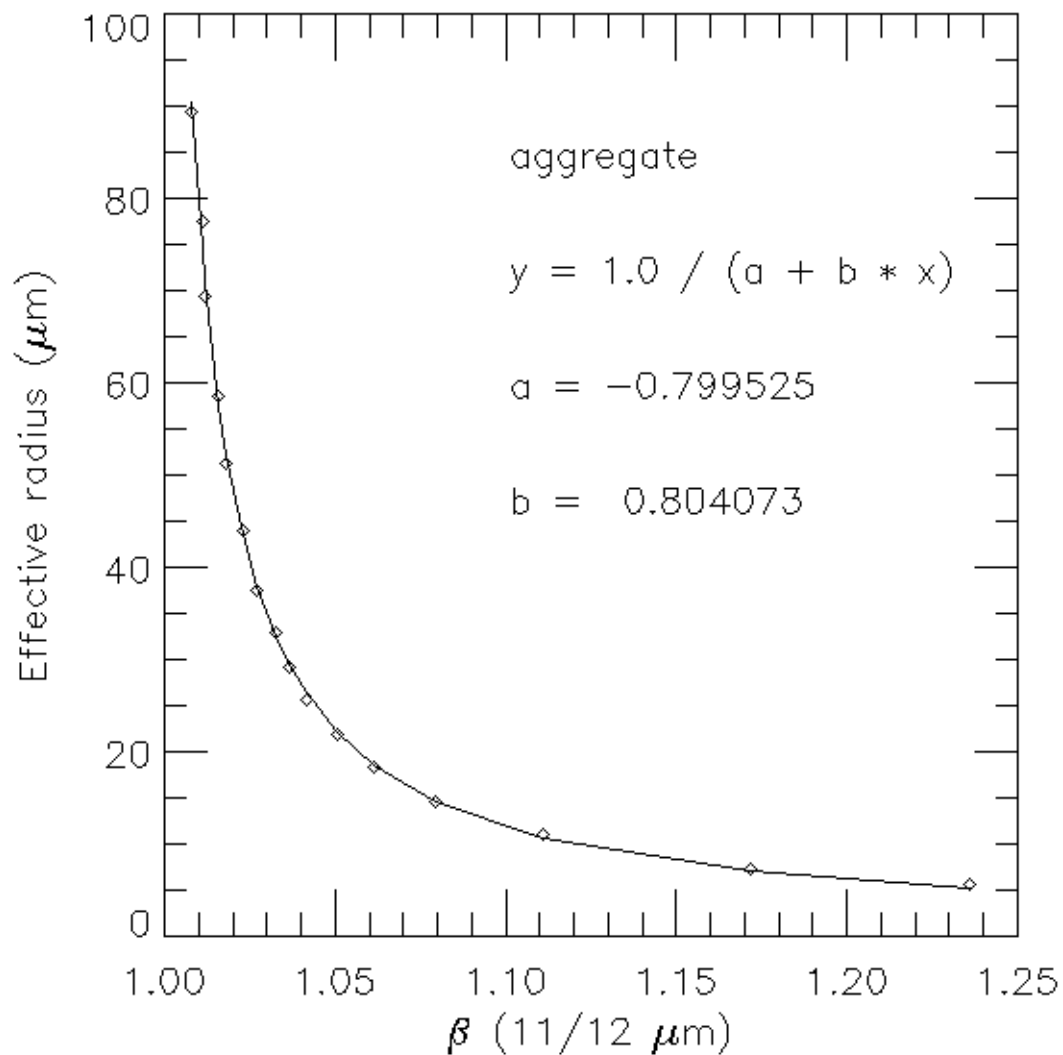
Figure 8: Variation of the 11 and 12 μm β values as a function of the ice crystal radius. This relation is used in the retrieval to produce an estimate of cloud particle size from the final retrieved β values.

3.4.1.3   Mathematical Description

The mathematical approach employed here is the optimal estimation approach described by Rodgers (1976). The optimal estimation approach is also often referred to as a 1DVAR approach. The benefits of this approach are that it is flexible and allows for the easy addition or subtraction of new observations or retrieved parameters. Another benefit of this approach is that it generates automatic estimates of the retrieval errors. The following description of the method employs the same notation as Rodgers (1976) but provides only a brief review.

The optimal estimation (3) approach minimizes a cost function, Φ, given by

$$\phi = (x - x_a)^T S_a^{-1}(x - x_a) + (y - f(x))^T S_y^{-1}(y - f(x)) \tag{6}$$

where **x** is a vector of retrieved parameters, **x$_a$** is a vector housing the a priori values of **x** (which also serve as a first guess to begin iterations to a convergent solution), **y** is the vector of observations, and **f** is the forward model's estimates of the values of **y** under the assumptions of state **x**. **S$_a$** is the error covariance matrix corresponding to the values of **x$_a$**, and **S$_y$** is the error covariance matrix for the forward model and measurements.

In each retrieval iteration, the state vector **x** is incremented as follows:

$$\delta x = S_x K^T S_y^{-1}[y - f(x)] + S_a^{-1}(x_a - x) \tag{7}$$

where **K** is the Jacobian or Kernel matrix (whose computation is described below) and **S$_x$** is the covariance error matrix of **x** which is computed as

$$S_x = (S_a^{-1} + K^T S_y^{-1} K)^{-1} \tag{8}$$

The retrieval iterations are conducted until the following criterion is met:

$$\left\| \sum \delta x S_x^{-1} \delta x \right\| \leq \frac{p}{2} \tag{9}$$

where **p** is the number of elements in **x**.

In ACHA, using mode 3, the **y** and **x** vectors are defined as follows:

$$y = \begin{pmatrix} BT(11\mu m) \\ BTD(11 - 12\mu m) \\ BTD(11 - 13.3\mu m) \end{pmatrix} \tag{10}$$

$$x = \begin{pmatrix} T_c \\ e(11\mu m) \\ \beta(12/11\mu m) \end{pmatrix} \tag{11}$$

$$x_a = \begin{pmatrix} T_c\_ap \\ e(11\mu m)\_ap \\ \beta(12/11\mu m)\_ap \end{pmatrix} \tag{12}$$

The Kernel matrix contains the partial derivatives of each element of **f(x)** to each element of **x**. In Heidinger and Pavolonis (2009), the equations defining all of the elements of **K** except those that involve the 13.3 μm channel are given. The following relationships repeat those in Heidinger and Pavolonis (2009) and provide the remaining terms used in the ACHA.

$$K = \begin{pmatrix} \dfrac{\partial BT(11\mu m)}{\partial T_{eff}} & \dfrac{\partial BT(11\mu m)}{\partial e(11\mu m)} & \dfrac{\partial BT(11\mu m)}{\partial \beta(12/11\mu m)} \\[2ex] \dfrac{\partial BTD(11-12\mu m)}{\partial T_{eff}} & \dfrac{\partial BTD(11-12\mu m)}{\partial e(11\mu m)} & \dfrac{\partial BTD(11-12\mu m)}{\partial \beta(12/11\mu m)} \\[2ex] \dfrac{\partial BTD(11-13.3\mu m)}{\partial T_{eff}} & \dfrac{\partial BTD(11-13.3\mu m)}{\partial e(11\mu m)} & \dfrac{\partial BTD(11-13.3\mu m)}{\partial \beta(12/11\mu m)} \end{pmatrix} \qquad (13)$$

The expressions required for the first column of **K** are given by Eqs. 14-16.

$$\frac{\partial BT(11\mu m)}{\partial T_c} = e_c(11\mu m)t_{ac}(11\mu m)\left(\frac{\partial B(11\mu m)}{\partial T_c}\right)\left(\frac{\partial B(11\mu m)}{\partial T}\right)^{-1} \qquad (14)$$

$$\frac{\partial BTD(11-12\mu m)}{\partial T_c} = \frac{\partial BT(11\mu m)}{\partial T_c} - e_c(12\mu m)t_{ac}(12\mu m)\left(\frac{\partial B(12\mu m)}{\partial T_c}\right)\left(\frac{\partial B(12\mu m)}{\partial T}\right)^{-1} \qquad (15)$$

$$\frac{\partial BTD(11-13.3\mu m)}{\partial T_{eff}} =$$
$$\frac{\partial BT(11\mu m)}{\partial T_c} - e_c(13.3\mu m)t_{ac}(13.3\mu m)\left(\frac{\partial B(13.3\mu m)}{\partial T_c}\right)\left(\frac{\partial B(13.3\mu m)}{\partial T}\right)^{-1} \qquad (16)$$

The expressions for the second column of **K** are given by Eqs. 17-19.

$$\frac{\partial BT(11\mu m)}{\partial e_c(11\mu m)} = [R_{cld}(11\mu m) - R_{clr}(11\mu m)]\left(\frac{\partial B(11\mu m)}{\partial T}\right)^{-1} \qquad (17)$$

$$\frac{\partial BTD(11-12\mu m)}{\partial e_c(11\mu m)} =$$
$$\frac{\partial BT(11\mu m)}{\partial e_c(11\mu m)} - [R_{cld}(12\mu m) - R_{clr}(12\mu m)][\beta(12/11\mu m)(1-e_c(11\mu m))^{\beta(12/11\mu m)-1}]\left(\frac{\partial B(12\mu m)}{\partial T}\right)^{-1} \qquad (18)$$

$$\frac{\partial BTD(11-13.3\mu m)}{\partial e_c(11\mu m)} =$$
$$\frac{\partial BT(11\mu m)}{\partial e_c(11\mu m)} - [R_{cld}(13.3\mu m) - R_{clr}(13.3\mu m)][\beta(13.3/11\mu m)(1-e_c(11\mu m))^{\beta(13.3/11\mu m)-1}]\left(\frac{\partial B(13.3\mu m)}{\partial T}\right)^{-1} \qquad (19)$$

Finally, the derivative of each forward model simulation with respect to $\beta(12/11\mu m)$ is given by the following equations:

$$\frac{\partial BT(11\mu m)}{\partial \beta(12/11\mu m)} = 0.0 \qquad (20)$$

$$\frac{\partial BTD(11-12\mu m)}{\partial \beta(12/11\mu m)} = [R_{cld}(12\mu m) - R_{clr}(12\mu m)]\ln[1 - e_c(11\mu m)][1 - e_c(12\mu m)]\left(\frac{\partial B(12\mu m)}{\partial T}\right)^{-1} \quad (21)$$

$$\frac{\partial BTD(11-13.3\mu m)}{\partial \beta(12/11\mu m)} =$$

$$[R_{cld}(13.3\mu m) - R_{clr}(13.3\mu m)]\ln[1 - e_c(11\mu m)][1 - e_c(13.3\mu m)]\left(\frac{\partial \beta(13.3/11\mu m)}{\partial \beta(12/11\mu m)}\right)\left(\frac{\partial B(13.3\mu m)}{\partial T}\right)^{-1}$$

$$(22)$$

The values of $\partial \beta_{11/13}\big/\partial \beta_{11/12}$ are computed using the regression shown in **Figure 6**.

For water clouds, the same form of a regression shown in **Figure 6** is used except that the a-coefficient is -0.217 and the b-coefficient is 1.250.

3.4.2   Data Merging Strategy

Not Applicable.

3.4.3   Numerical Strategy

The ACHA uses only infrared observations in order to provide products that are consistent for day, night and terminator conditions. The ACHA uses an analytical model of infrared radiative transfer imbedded into an optimal estimation retrieval methodology (1DVAR, Rogers 1976). Cloud-top pressure and cloud-top height are derived from the cloud-top temperature product and the atmospheric temperature profile provided by Numerical Weather Prediction (NWP) data.

The ACHA uses the spectral information provided by the satellite imager to derive cloud-top height information simultaneously with cloud microphysical information. Table 3 lists the currently available ACHA "modes" and respective channel combinations. This information allows the ACHA to avoid making assumptions on cloud microphysics in the retrieval of cloud height. As a consequence, ACHA also generates the intermediate products of 11 μm cloud emissivity and an 11/12, or 11/13.3, or 11/8.5, or 11/6.7 μm microphysical index.

3.4.4   Calculations

Not Applicable.

3.4.5   Look-Up Table Description

Many of the a priori constants are contained in the "awg_cld_hght_include_1.inc", "acha_water_cloud_microphysical_model.inc", and "acha_ice_cloud_microphysical_model.inc" files that are supplied with the software delivery.

Table 4: The a priori (first guess) retrieval values used in the ACHA. Columns shown are a priori cloud temperature, uncertainty in cloud temperature, cloud emissivity, emissivity uncertainty, β and its uncertainty, and transmittance.

Cloud Type	T_c	$\sigma(T_c)$	ε	$\sigma(\varepsilon)$	β	$\sigma(\beta)$	τ
Fog	BT(11μm)	10 K	0.7	0.1	1.3	0.2	1.2
Water	BT(11μm)	10 K	0.9	0.1	1.3	0.2	2.3
Supercooled	BT(11μm)	10 K	0.9	0.1	1.3	0.2	2.3
Mixed	BT(11μm)	10 K	0.9	0.1	1.3	0.2	2.3
Thick Ice	BT(11μm)	10 K	0.9	0.1	1.06	0.2	2.3
Cirrus	T(tropo) – 15 K	20 K	0.6	0.4	1.06	0.2	0.9
Multi-layer	T(tropo) – 15 K	20 K	0.6	0.4	1.06	0.2	2.0

Table 5: Values of uncertainty (K) for the forward model used in the ACHA retrieval. BTD is the brightness temperature difference.

Element of f	σ_{inst}	σ_{clear}(Ocean)	σ_{clear}(Land)
T(11 μm)	1.0	1.5	5.0
BTD(11 – 12 μm)	0.5	0.5	1.0
BTD(11 – 13.3 μm)	1.0	0.5	1.0
BTD(11 – 8.5 μm)	0.5	0.5	1.0
BTD(11 – 6.7 μm)	1.0	0.5	1.0

Table 6: Mean calculated clear sky brightness temperatures (K) for surface type and wavelength.

Surface Type	BT(6.7 μm)	BT(8.5 μm)	BT(11 μm)	BT(12 μm)	BT(13.3 μm)
Water	237.175	285.360	287.384	285.908	265.054
Land	236.521	285.905	287.907	286.094	265.588
Snow	216.762	247.841	252.854	252.213	235.644
Desert	205.415	226.472	228.628	228.141	218.694
Arctic	223.444	261.708	268.111	266.699	247.740
Antarctic	216.762	247.841	252.854	252.213	235.644

Table 7: Calculated clear sky brightness temperature (K) covariance terms for each surface type.

Surface Type	cov(6.7, 6.7 μm)	cov(8.5, 8.5 μm)	cov(11, 11 μm)	cov(12, 12 μm)	cov(13.3, 13.3 μm)
Water	13.865	2.656	1.603	1.830	0.818
Land	10.979	29.028	34.016	31.408	4.869
Snow	7.450	33.423	32.312	32.714	9.407
Desert	12.948	44.966	53.745	50.583	6.422
Arctic	2.916	18.341	20.321	19.717	4.462
Antarctic	7.823	34.741	34.387	33.899	17.091

Table 8: Calculated clear sky brightness temperature (K) covariance terms for the 0.67 μm channel and each surface type.

Surface Type	cov(11, 6.7 μm)	cov(12, 6.7 μm)	cov(6.7, 13.3 μm)
Water	0.831	1.035	1.129
Land	0.504	0.807	1.207
Snow	1.016	1.070	1.234
Desert	-0.334	0.024	1.045
Arctic	0.328	0.346	0.469
Antarctic	10.187	10.159	7.746

Table 9: Calculated clear sky brightness temperature differences (K) covariance terms for the 0.67 μm channel and each surface type. Square brackets represent BTD between channels.

Surface Type	cov([11, 6.7], [11, 6.7])	cov([11, 12], [11, 6.7])	cov([11, 6.7], [11, 13.3])
Water	13.806	0.127	1.088
Land	43.987	1.821	23.936
Snow	37.732	-0.117	15.574
Desert	67.362	2.254	39.489
Arctic	22.581	0.346	11.400
Antarctic	21.836	0.231	8.255

Table 10: Calculated clear sky brightness temperature (K) covariance terms for the 0.85 µm channel and each surface type.

Surface Type	cov(8.5, 13 µm)	cov(11, 8.5 µm)	cov(12, 8.5 µm)
Water	0.732	1.450	1.493
Land	9.772	30.984	29.487
Snow	16.397	31.103	31.286
Desert	13.737	44.917	42.656
Arctic	8.650	19.159	18.848
Antarctic	23.931	34.512	34.256

Table 11: Calculated clear sky brightness temperature differences (K) covariance terms for the 0.85 µm and each surface type. Square brackets represent BTD between channels.

Surface Type	cov([11, 8.5], [11, 8.5])	cov([11, 12], [11, 8.5])
Water	1.360	-0.033
Land	1.078	0.021
Snow	3.530	0.011
Desert	8.880	-0.365
Arctic	0.344	0.017
Antarctic	0.104	0.004

Table 12: Calculated clear sky brightness temperature (K) covariance terms for the 12 µm channel and each surface type.

Surface Type	cov(12, 13 µm)	cov(12, 8.5 µm)	cov(12, 6.7 µm)	cov(11, 12 µm)
Water	0.956	1.493	1.035	1.679
Land	10.814	29.487	0.807	32.499
Snow	17.089	31.286	1.070	32.484
Desert	15.616	42.656	0.024	51.851
Arctic	8.967	18.848	0.346	19.993
Antarctic	23.518	34.256	10.159	34.128

Table 13: Calculated clear sky brightness temperature differences (K) covariance terms for the 12 μm channel and each surface type. Square brackets represent BTD between channels.

Surface Type	cov([11, 12], [11, 12])	cov([11, 12], [11, 13])	cov([11, 12], [11, 8.5])	cov([11, 12], [11, 6.7])
Water	0.075	0.067	-0.033	0.127
Land	0.427	1.548	0.021	1.821
Snow	0.057	-0.041	0.011	-0.117
Desert	0.629	1.875	-0.365	2.254
Arctic	0.052	0.233	0.017	0.346
Antarctic	0.030	0.086	0.004	0.231

Table 14: Calculated clear sky brightness temperature (K) covariance terms for the 13.3 μm channel and each surface type.

Surface Type	cov(11, 13 μm)	cov(8.5, 13 μm)	cov(12, 13 μm)	cov(6.7, 13 μm)
Water	0.813	0.732	0.956	1.129
Land	10.784	9.772	10.814	1.207
Snow	16.957	16.397	17.089	1.234
Desert	15.636	13.737	15.616	1.045
Arctic	9.062	8.650	8.967	0.469
Antarctic	23.691	23.931	23.518	7.746

Table 15: Calculated clear sky brightness temperature differences (K) covariance terms for the 13.3 μm channel and each surface type. Square brackets represent BTD between channels.

Surface Type	cov([11, 13], [11, 13])	cov([11, 12], [11, 13])	cov([11, 6.7], [11, 13])
Water	0.796	0.067	1.088
Land	17.318	1.548	23.936
Snow	7.804	-0.041	15.574
Desert	28.896	1.875	39.489
Arctic	6.658	0.233	11.400
Antarctic	4.096	0.086	8.255

Table 16: Calculated clear sky brightness temperature (K) covariance terms for the 11 μm channel and the brightness temperature differences for each surface type.

Surface Type	cov([11], [11, 12])	cov([11,], [11, 6.7])	cov([11], [11, 8.5])	cov([11], [11, 13])
Water	-0.076	0.772	0.154	0.791
Land	1.518	33.514	3.033	23.233
Snow	-0.172	31.297	1.209	15.355
Desert	1.895	54.080	8.829	38.110
Arctic	0.328	19.993	1.162	11.259
Antarctic	0.259	24.200	-0.125	10.696

Table 17: Mie theory (water clouds) computed linear fit (y = a + b*x) of the β values of the spectral combination shown in the table to those computed using the 11/12 μ β.

Spectral combination	a	b
11/6.7 μm	0.268115	0.702683
11/8.5 μm	0.930569	0.048857
11/13.3 μm	-0.728113	1.743389

Table 18: Ice clouds modeled as aggregate columns' computed linear fit (y = a + b*x) of the β values of the spectral combination shown in the table to those computed using the 11/12 μ β.

Spectral combination	a	b
11/6.7 μm	0.95539	0.07902
11/8.5 μm	1.40457	-0.39163
11/13.3 μm	-0.02641	1.08386

Table 19: β fit parameters used in effective radius calculations.

Effective Radius (μm)	A	B	C	D
Ice Model	-8.46300	18.82502	-13.19113	3.34004
Water Model	TBD	TBD	TBD	TBD

Table 20: 11 μm asymmetry fit parameters, used in the calculation of asymmetry.

Asymmetry Parameter	A	B	C
Ice Model (11 μm)	0.64054	0.37904	-0.10336
Water Model (11 μm)	TBD	TBD	TBD

Table 21: 11 μm single scattering albedo fit parameters, used in the calculation of the single scattering albedo.

Single Scattering Albedo	A	B	C
Ice Model (11 μm)	0.00705	0.59694	-0.16978
Water Model (11 μm)	TBD	TBD	TBD

Table 22: 11 μm extinction fit parameters, used in the calculation of the extinction coefficient.

Extinction Coefficient	A	B	C
Ice Model (11 μm)	-0.34298	2.42808	-0.63351
Water Model (11 μm)	TBD	TBD	TBD

Table 23: 0.65 μm extinction fit parameters, used in the calculation of the extinction coefficient.

Extinction Coefficient	A	B	C
Ice Model (.65 μm)	2.25389	-0.23436	0.05582
Water Model (.65 μm)	TBD	TBD	TBD

3.4.6   Parameterization

3.4.6.1   Estimation of Prior Values and their Uncertainty

The proper implementation of ACHA requires meaningful estimates of *a priori* values housed in x_a and their uncertainties housed in S_a. S_a is a two-dimensional matrix with each dimension being the size of x_a. For the ACHA, we assume S_a is a diagonal matrix with each element being the assumed variance of each element of x_a as illustrated below.

$$S_a = \begin{pmatrix} \sigma^2_{Tc\_ap} & 0.0 & 0.0 \\ 0.0 & \sigma^2_{\varepsilon c(11\mu m)\_ap} & 0.0 \\ 0.0 & 0.0 & \sigma^2_{\beta(12/11\mu m)\_ap} \end{pmatrix} \qquad (23)$$

In the ACHA, we currently use the *a priori* estimate of x_a and S_a given by Heidinger and Pavolonis (2009). In this paper, CALIPSO-derived values of T_c, e_c, and β are derived, and distributions are computed for the various cloud types generated by the cloud-typing algorithm. The means and standard deviations of these distributions are used for the values of x_a and S_a for the non-opaque cloud types (cirrus and multi-layer). For the opaque cloud types, the *a priori* values of T_c are provided by the 11 μm brightness temperature. The *a priori* values of β are taken from scattering theory and are set to 1.1 for ice-phase clouds and 1.3 for water-phase clouds. The standard deviation of β is assumed to be 0.2 based on the distributions of Heidinger and Pavolonis (2009).

3.4.6.2   Estimation of Forward Model Uncertainty

This section describes the estimation of the elements of S_y, which contain the uncertainty expressed as a variance of the forward model estimates. As was the case with S_a, S_y is assumed be a diagonal matrix. As our experience with the ACHA grows, the computation of the off-diagonal will be explored.

Assumed to be diagonal, S_y can be expressed as follows:

$$S_y = \begin{pmatrix} \sigma^2_{BT(11\mu m)} & 0.0 & 0.0 \\ 0.0 & \sigma^2_{BTD(11-12\mu m)} & 0.0 \\ 0.0 & 0.0 & \sigma^2_{BTD(11-13.3\mu m)} \end{pmatrix} \qquad (24)$$

The variance terms are computed by summing up three components:

$$\sigma^2 = \sigma^2_{instr} + [1 - e_c(11\mu m)]\sigma^2_{clr} + \sigma^2_{hetero} \qquad (25)$$

The first component (σ^2_{instr}) represents instrument noise and calibration uncertainties. The second component represents uncertainties caused by the clear-sky radiative transfer (σ_{clear}). σ_{clear} is assumed to decrease linearly with increasing e_c. For opaque clouds, the uncertainties associated with clear-sky radiative transfer are assumed to be negligible. Due to the large variation in NWP biases on land and ocean, separate land and ocean uncertainties are assumed. The third component (σ_{hetero}) is the term that accounts for the larger uncertainty of the forward model in regions of large spatial heterogeneity. Currently, the ACHA uses the standard deviation of each element of y computed over a 3x3 pixel array as the value of σ_{hetero}. **Table 4** provides the current values used for the instrumental and clear-sky terms in constructing S_y.

3.4.6.3   Estimation of Quality Flags and Errors

One of the benefits of the 1DVAR approach is the diagnostic terms it generates automatically. If the values of S_a, S_y and K are properly constructed, the values of S_x should provide an estimate of the uncertainties of the retrieved parameters, x. The diagonal term of S_x provides the uncertainty expressed as a variance of each parameter. While these estimates are useful, the current ACHA also generates a 4-level quality flag. The integer quality flags are determined by the relative values of the diagonal terms of S_x and S_a. If the estimated uncertainty in a element of x is less than one third of the prescribed uncertainty of the corresponding element of x_a, a parameter quality indicator, which is not the product quality flag described in section 3.4.7.3, of 3 is assigned. Similarly a parameter quality indicator of 2 is assigned for pixels where the estimated uncertainty of x lies between one third and two thirds of the uncertainty of the corresponding element of x_a. Values with higher uncertainties are given a parameter quality indicator of 1.   Retrievals that do not converge are given a parameter quality indicator of 0. A description of the parameter quality indicator is in section 3.4.7.2.

3.4.6.4   Impact of Local Radiative Center Pixels

As discussed above, the first pass through the retrieval occurs for those pixels determined to be local radiative centers, which physically correspond to local maxima in cloud opacity. The full pixel processing order is described below. The objective is to first apply the retrieval to the more opaque pixels and to use this information for the less opaque pixels. In the ACHA, the *a priori* value of T_c for pixels that have local radiative centers identified for them are assumed to be the values of T_c estimated for the local radiative centers. The uncertainty of the *a priori* T_c values remains those given in **Table 5**.

3.4.6.5   Treatment of Multi-layer Clouds

For pixels determined to be multi-layer clouds, the lower boundary condition is assumed to be a lower cloud and not the surface of the earth. With this assumption, the forward model remains unchanged when treating multi-layer clouds. As discussed by Heidinger and Pavolonis (2009), the mean height of water clouds determined from MODIS is 2 km above the surface. Therefore, for all multi-layer pixels, the lower boundary condition is assumed to be an opaque cloud situated 2 km above the surface of the earth. The same equations apply except that the clear-sky observations are recomputed to reflect the change in the lower boundary condition. It is a goal for future versions of this algorithm to dynamically compute the height/temperature of the lower cloud layer in multi-layer situations.

In the ACHA, information about the height of the surrounding low clouds is used to estimate the height of low clouds underneath higher clouds in detected multi-layer situations. **Figure 9** provides a visual aid for understanding this process.   In this example, assume that the imager pixel observed above Low Cloud #3 is correctly identified as a multi-layer cloud by the cloud typing algorithm. Also, assume that Low Clouds #1 and #5 are correctly identified as low clouds and have successful cloud height solutions from the ACHA.   The ACHA uses the height information for Low Clouds #1 and #5 to estimate the

height of Low Cloud #3 instead of assuming a fixed height of all low clouds detected below high clouds. This computation is accomplished by taking the mean of all low cloud pressures that surround the multi-layer cloud pixel within a *NxN* box. Currently, the size of the box (*N*) is set to 5. This variable is a configurable parameter (INTERP_LOWER_CLOUD_PIXEL_RADIUS). If no low cloud results are found within the *NxN* box, a default value of the cloud pressure is used. This default value is 200 hPa lower than the surface pressure.   The application of this logic requires that the low cloud information be available before processing the multi-layer pixels. This logic is described in the next section.
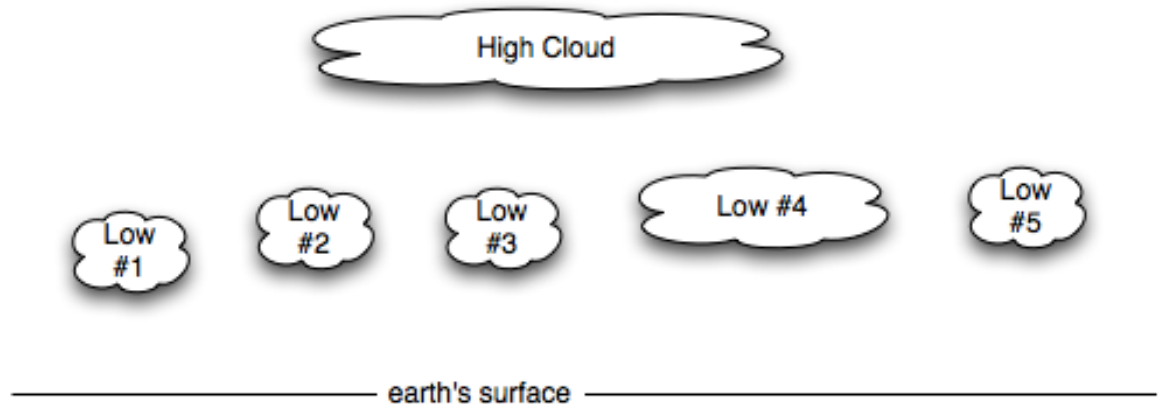
Figure 9: Schematic illustration of mulit-layer clouds.

3.4.6.6   Pixel Processing Order with the ACHA

As stated above, applying the multi-layer logic and applying local-radiative center logic require that some pixels be processed before others. In this section, we describe this logic. The pixel processing order in the ACHA is as follows:

1. Single-layer Radiative Centers,

2. Non-local radiative center water clouds,

3. Multi-layer clouds, and

4. All remaining unprocessed cloudy pixels.

Pixels that are single-layer radiative centers can be done first since they rely on the results of no other pixels. Pixels that are single-layer water clouds can then be processed because they would be influenced by the pixels that are single layers and radiative centers. Single-layer ice pixels cannot be processed yet since they may require knowledge of the multi-layer results if their LRC computation points to a multi-layer pixel. The next pixels that can be processed are the multi-layer pixels. After this computation, all remaining pixels can be processed.

3.4.6.7   Computation of Cloud Height and Cloud Pressure

Once T_c is computed, the NWP temperature profiles are used to interpolate the values of cloud-top pressure, P_c, and cloud-top height, Z_c. Two separate methods are applied depending on whether the cloud is in an inversion or not. An inversion is defined as a region in the atmosphere where the temperature increases with height. **Figure 10** provides an illustration of an inversion. When a cloud temperature is found to reside outside of an inversion, a simple linear interpolation is used to estimate cloud-top pressure and height. In the presence of inversions, the monotonic relationship between temperature and pressure/height disappears and a single value of cloud temperature can correspond to multiple pressure or height values. Atmospheric inversions are common at low levels over the ocean. This issue plagues all infrared cloud height algorithms including those employed by the MODIS and GOES sounder teams.

The presence of low-level inversions is determined by analysis of the NWP temperature profile. Currently, if any layer below 700 hPa and 50 hPa above the surface is found to be warmer than the layer below it, the clouds are assumed to reside in an inversion as illustrated in **Figure 10**. In this case, the cloud height is estimated by dividing the difference between the cloud temperature and the surface temperature by a predefined lapse rate. Currently, the lapse rate is assumed to be the dry adiabatic value of -9.8 K/ km. The vertical resolution of NWP profiles is not sufficient to use them directly in the presence of inversions. This procedure is only implemented over water surfaces and for water-phase clouds.

It is important to note that this issue requires further study. The Cloud Application Team is working with the DMW team and other cloud remote sensing groups to determine an optimal strategy when inversions are present.
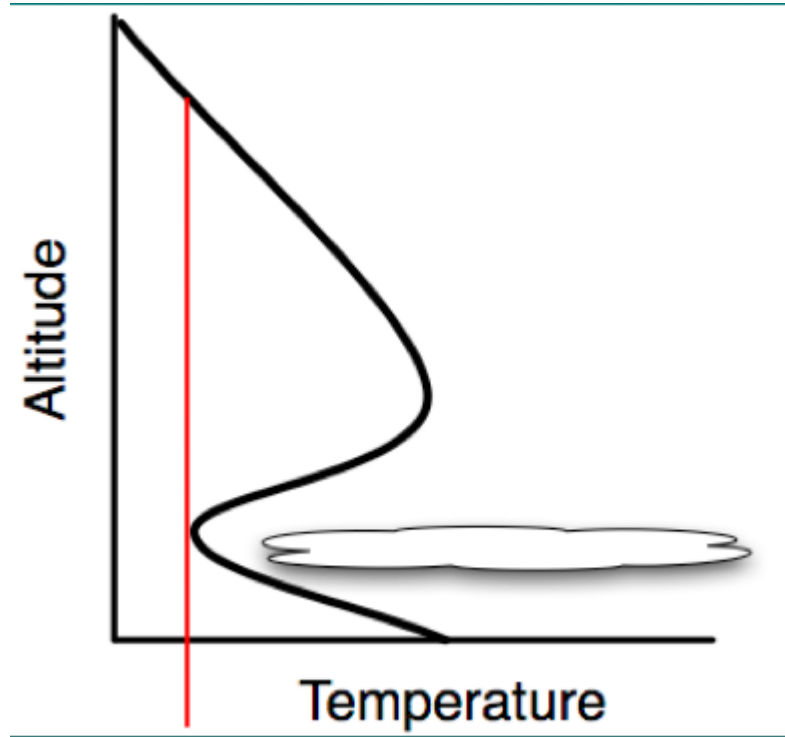
Figure 10: Illustration of a cloud located in a temperature inversion. (Figure provided by Bob Holz of UW/SSEC).

3.4.7 Algorithm Output

3.4.7.1 Output

The output of the ACHA provides the following cloud products listed in the F&PS:

- Cloud-top temperature,

- Cloud-top pressure, and

- Cloud-top height.

All of these products are derived at the pixel level for all cloudy pixels. Example images of the above products are provided in section 4.1.

3.4.7.2 Intermediate Data

The ACHA derives the following intermediate products that are not included in F&PS, but are used in other algorithms, such as the derived motion winds (DMW) algorithm:

- Error estimates,

- Cloud 11 $\Box$m emissivity, and

- Cloud microphysical index ($\Box$).

- Parameter Quality Indicator

The Parameter Quality Indicator is a discretized and normalized version of the error estimates. It is not a substitute for the product quality flag (see below). A detailed description of the parameter quality indicator is provided in section 3.4.6.3. Descriptions of all variables in the level2b file are included in Appendix B.

3.4.7.3 Product Quality Flag

In addition to the algorithm output, a pixel level product quality flag will be assigned. The possible values are as follows:

Table 24: Potential quality flags from ACHA.

Flag Value	Description
0	Valid, good quality converged retrieval
1	Invalid pixel due to space view
2	Invalid pixel due to being outside of sensor zenith range
3	Invalid earth pixel due to bad data (bad or missing 11 μm BT or bad/missing clear sky 11 μm BT)
4	Invalid due to cloud mask being clear or probably clear
5	Invalid due to missing cloud type
6	Failed retrieval

3.4.7.4 Processing Information Flag

In addition to the algorithm output and quality flags, processing information, or how the algorithm was processed, will be output for each pixel. If the bit is 0, then the answer was no, and if the bit is 1, the answer is yes.

Table 25: Processing information flags from ACHA.

Bit	Description
0	Cloud Height Attempted
1	Bias Correction Employed
2	Ice cloud retrieval
3	Local Radiative Center Processing Used
4	Multi-layer Retrieval
5	Lower Cloud Interpolation used
6	Boundary Layer Inversion Assumed

3.4.7.5   Metadata

In addition to the algorithm output, the following will be output to the file as metadata for each file:

- Mean, Min, Max and standard deviation of cloud top temperature;

- Mean, Min, Max and standard deviation of cloud top pressure;

- Mean, Min, Max and standard deviation of cloud top height;

- Number of QA flag values;

- For each QA flag value, the following information is required:

  o   Number of retrievals with the QA flag value,

  o   Definition of QA flag,

  o   Total number of detected cloud pixels, and

  o   Terminator mark or determination.

4. Test Datasets and Outputs

4.1 Test Input Datasets

As described below, the data used to test the ACHA include SEVIRI (imager on MSG) observations collocated with CALIPSO data. Data from August 2006 (summer), February 2007 (winter), April 2007 (spring) and October 2007 (fall) were used to span the entire SEVIRI domain and encompass a full range of conditions.

While SEVIRI does not operate over the GOES domains, we have felt more comfortable using SEVIRI/CALIPSO data than simulated ABI data up to this point. The rest of this section describes the proxy and validation datasets used in assessing the performance of the ACHA. **Table 26** shows the channel mapping between the proxy dataset (SEVIRI) and the ABI.

Table 26: Channel numbers and wavelengths for ABI.

ABI Channel Number	SEVIRI Channel Number	Wavelength (µm)
10	6	7.4
13	N/A	10.35
14	9	11.2
15	10	12.3
16	11	13.3

4.1.1 SEVIRI Data

SEVIRI provides 11 spectral channels with a spatial resolution of approximately 3 km and a temporal resolution of 15 minutes. SEVIRI provides the best source of data currently for testing and developing the ACHA. **Figure 11** shown below, is a full-disk SEVIRI image from 12 Z on August 10, 2006. Except for the 1.38 µm channel, SEVIRI provides an adequate source of proxy data for testing and developing the ACHA. Data from August 2006 (summer), February 2007 (winter), April 2007 (spring) and October 2007 (fall) were used to span the entire SEVIRI domain and encompass a full range of conditions. The SEVIRI data were provided by the UW/SSEC Data Center and processed for the datasets specified in section 4.1.
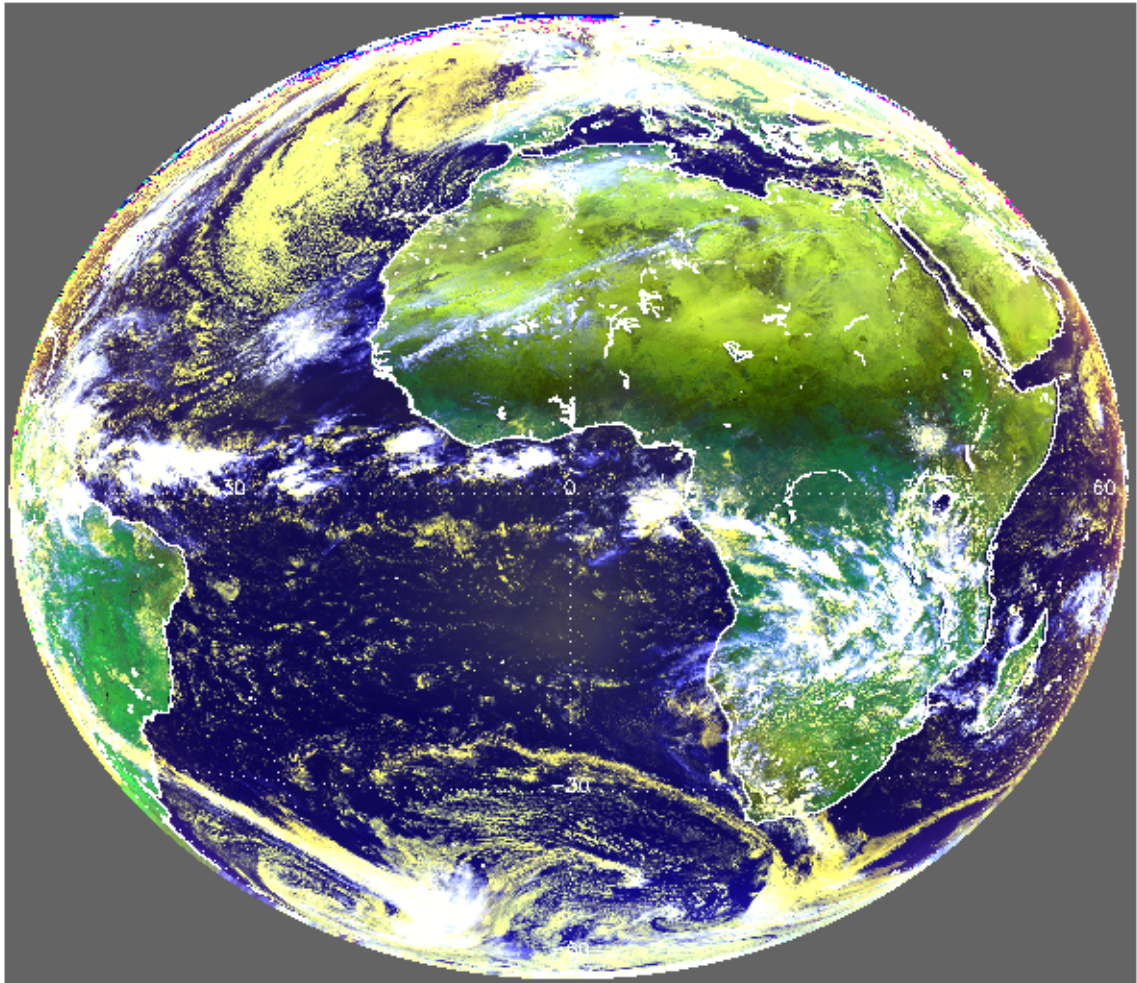
Figure 11: Full disk 0.63, 0.86 and 11 μm false color image from SEVIRI for 12 UTC on January 17, 2006.

4.1.1.1   CALIPSO Data

With the launch of CALIPSO and CloudSat into the NASA EOS A-Train in April 2006, the ability to conduct global satellite cloud product validation increased significantly. Currently, CALIPSO cloud layer results are being used to validate the cloud height product of the ACHA. The CALIPSO data used here are the 1 km cloud layer results.
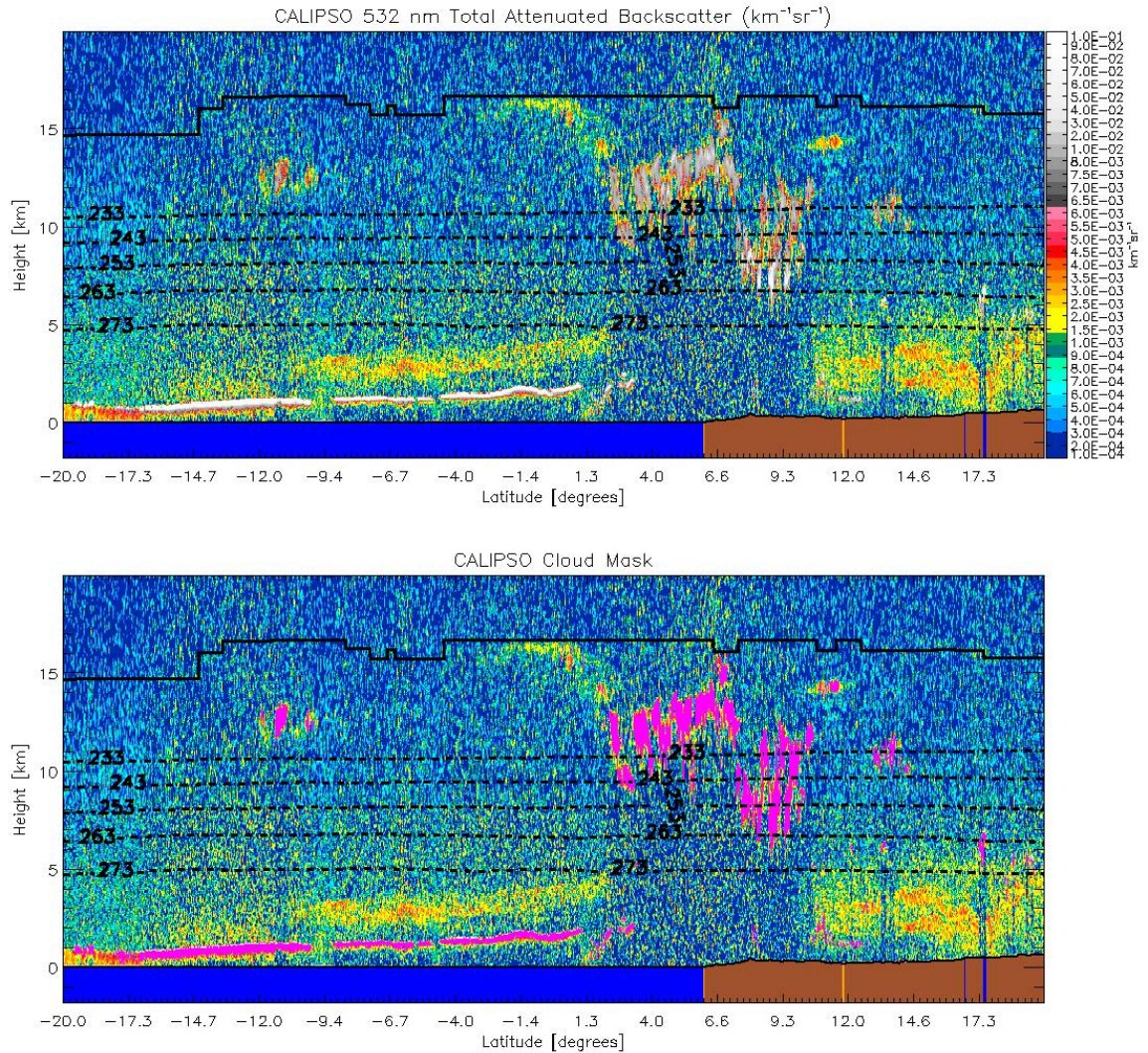
Figure 12: Illustration of CALIPSO data used in this study. Top image shows a 2D backscatter profile. Bottom image shows the detected cloud layers overlaid onto the backscatter image. Cloud layers are colored magenta. (Image courtesy of Michael Pavolonis, NOAA).

4.2   Test Output Analysis

4.2.1   Reproducibility

4.2.1.1   SEVIRI Example

The ACHA result was generated using the SEVIRI data from the dataset specified in section 4.1. During both the TRR and subsequent tests, comparisons between the online and offline (Cloud AWG) output of the ACHA, when the same inputs were used, showed an exact match of the height, temperature and pressure outputs. These tests were conducted under different conditions using the same input for both the online and offline tests. The

figures shown below illustrate the ACHA cloud-top temperature, height, pressure, and cloud emissivity. These images correspond to 12 Z on January 17, 2006 and correspond to the false-color image shown above. This day was chosen since it was also used in a recent EUMETSAT SEVIRI cloud product comparison workshop.
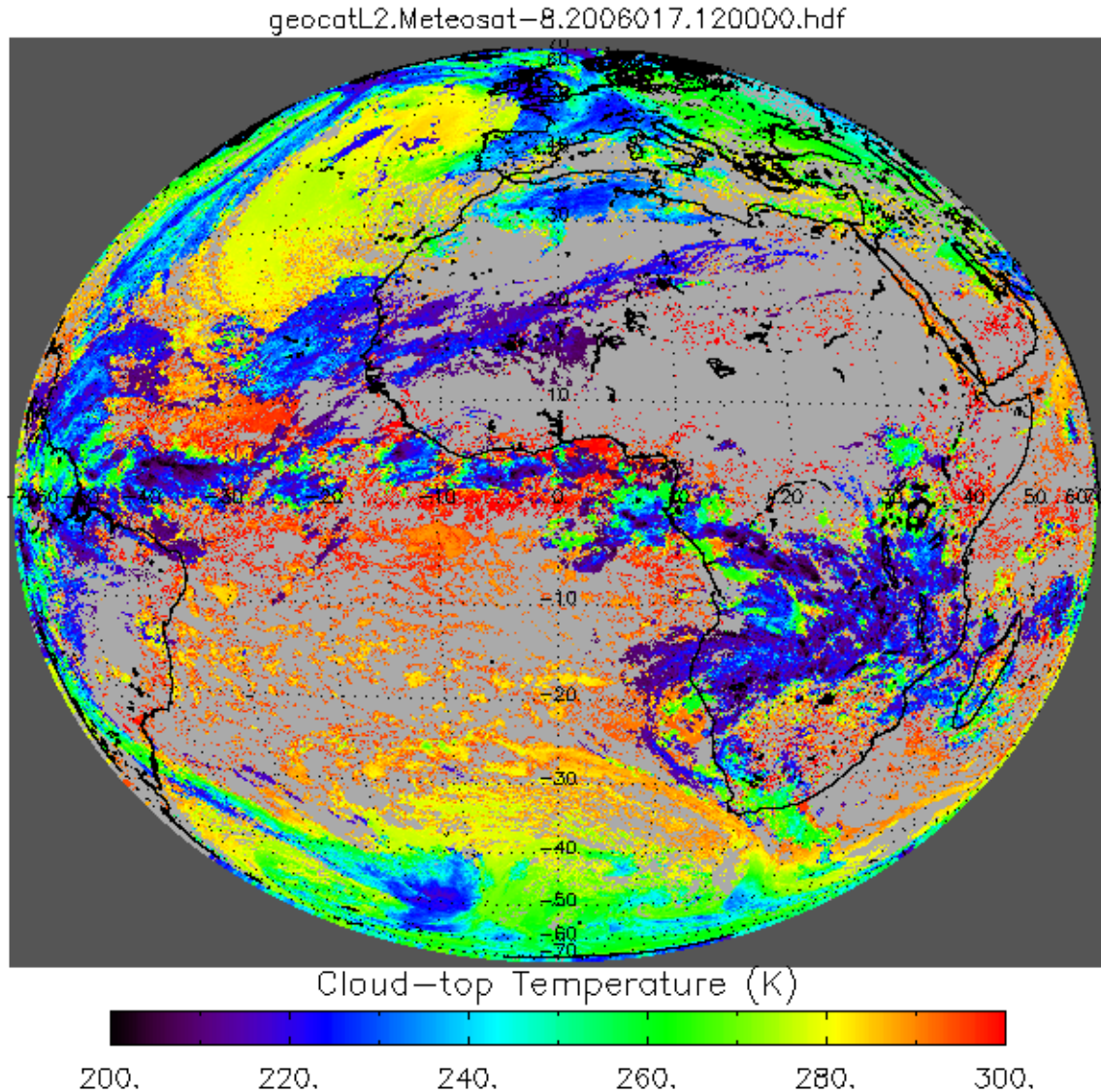
Figure 13: Example ACHA output of cloud-top temperature derived from SEVIRI proxy data for January 17, 2006.

geocatL2.Meteosat-8.2006017.120000.hdf

Cloud-top Pressure (hPa)

100.   280.   460.   640.   820.   1000.
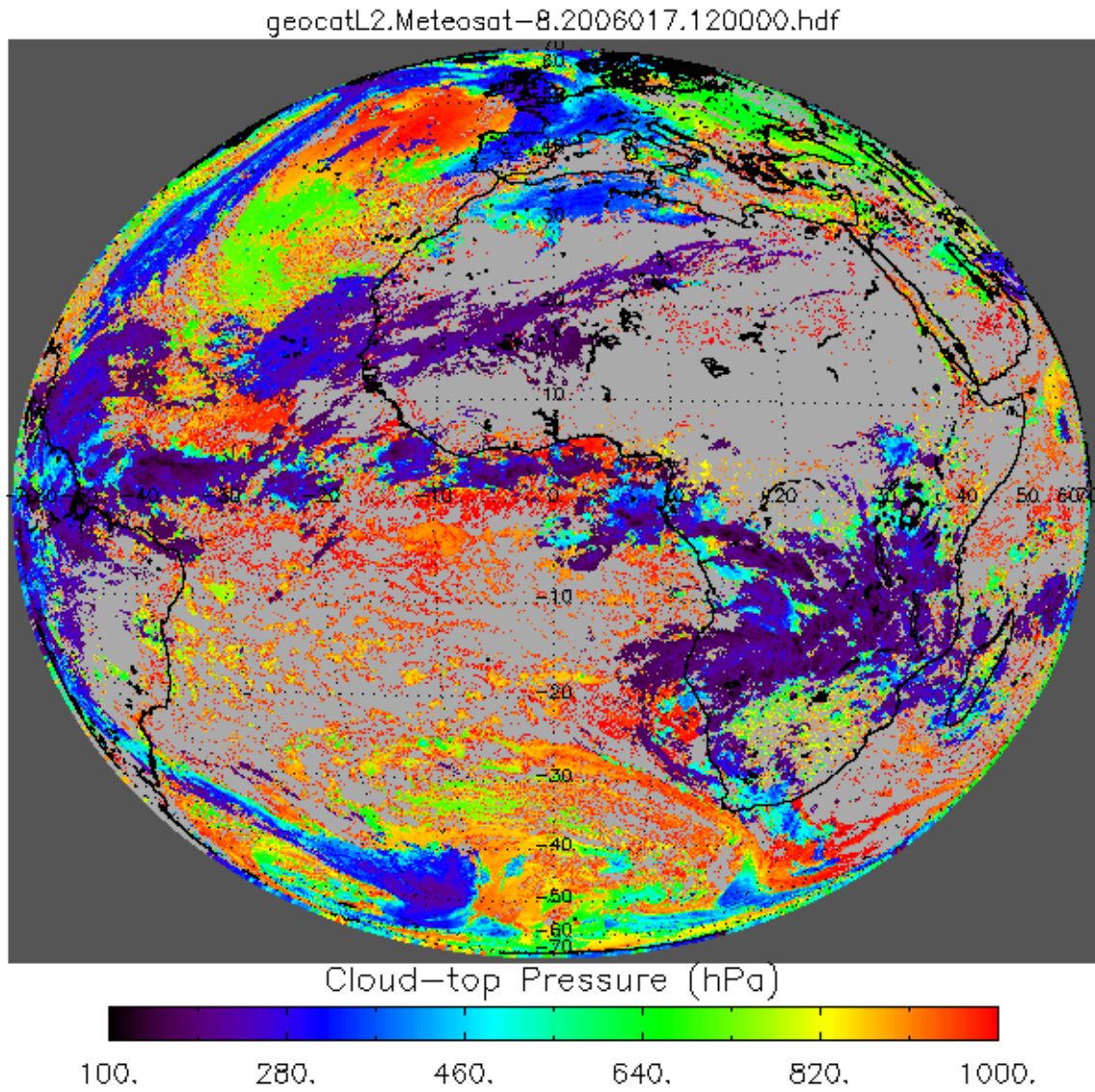
Figure 14: Example ACHA output of cloud-top pressure derived from SEVIRI proxy data for January 17, 2006.

geocatL2.Meteosat−8.2006017.120000.hdf

Cloud−top Height (m)

0.   3000.   6000.   9000.   12000.   15000.
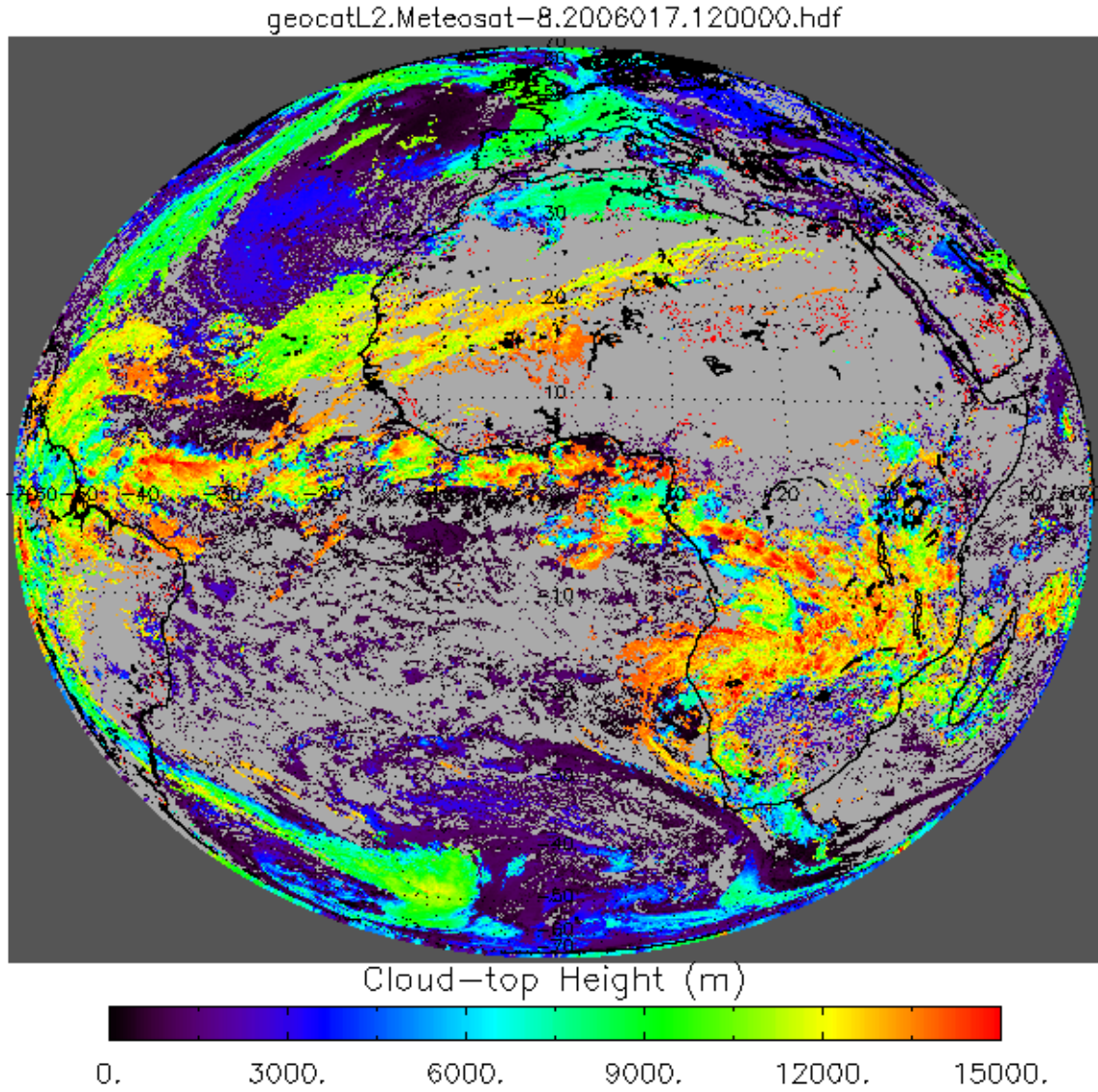
Figure 15: Example ACHA output of cloud-top height derived from SEVIRI proxy data for January 17, 2006.
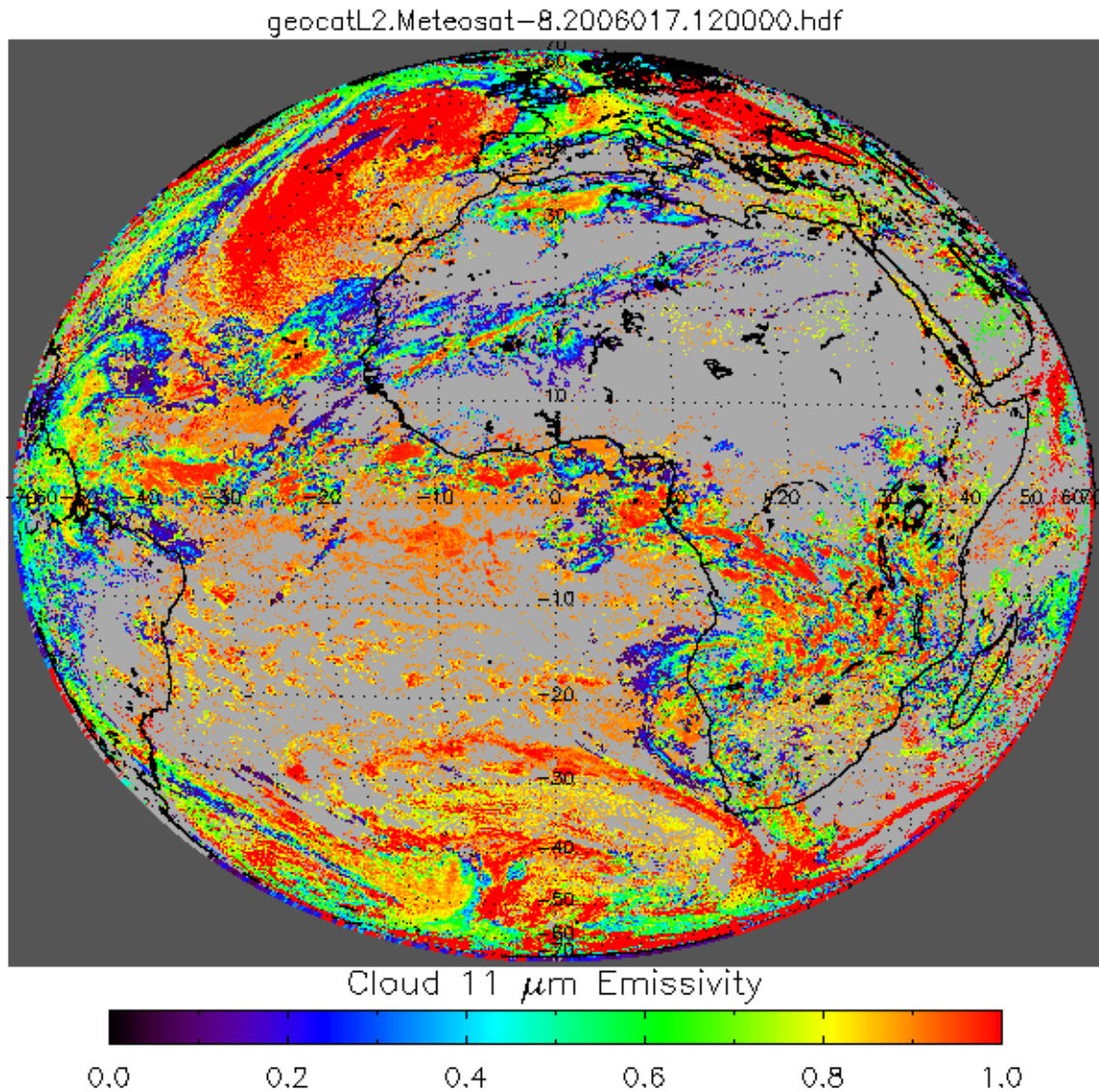
Figure 16: Example ACHA output of the 11µm cloud emissivity derived from SEVIRI proxy data for January 17, 2006.

4.2.1.2   PATMOS-x AVHRR Climate Level2b Example

The ACHA results in the subsequent images were generated using NOAA-18 data from September 1, 2005. The orbits contained in the level2b data set, and shown below, contain all ascending data for that day. The figures illustrate the ACHA cloud-top temperature, height, pressure, and cloud emissivity.

patmosx_noaa-18_asc_2005_244.level2b
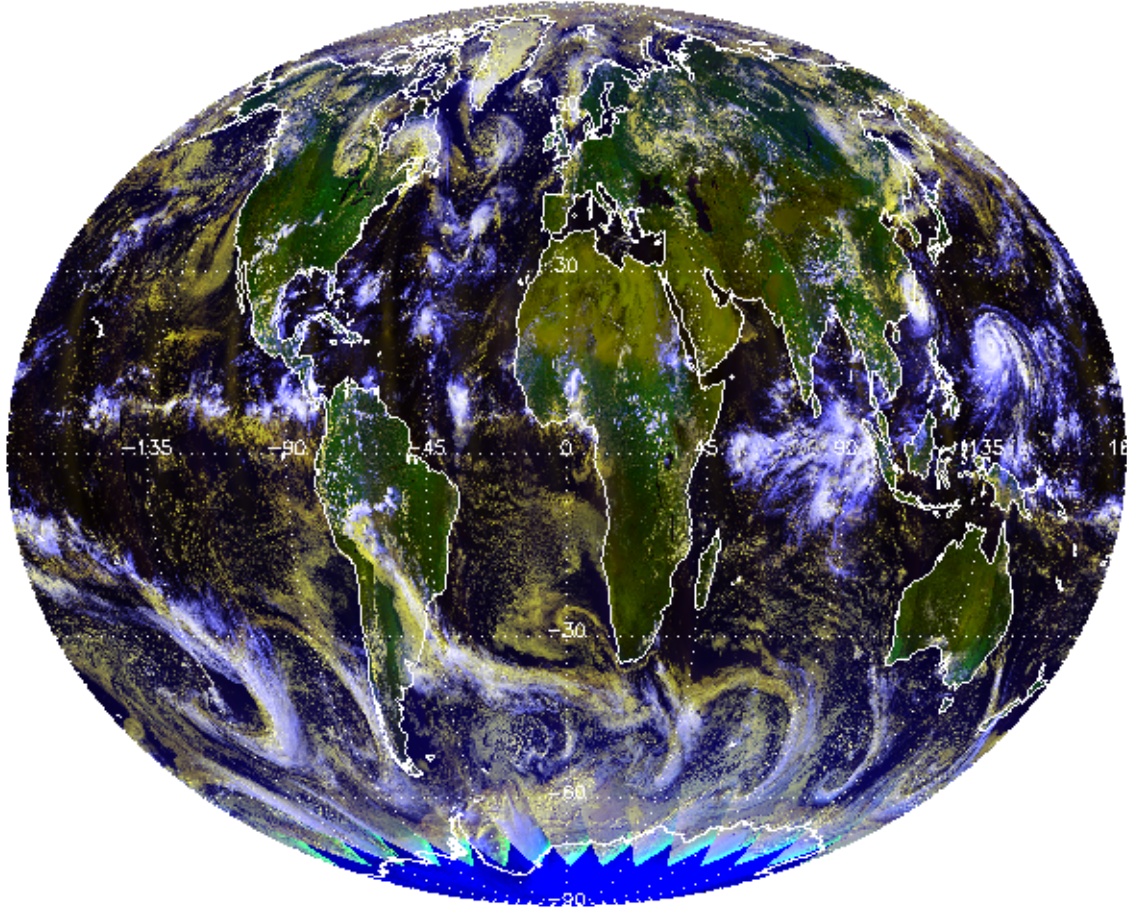
False Color Image

Red=0.63μm, Green = 0.86μm, Blue = 11μm (reversed)

Figure 17: NOAA-18 AVHRR 0.63, 0.86 and 11 μm (reversed) false color image from September 1, 2005.
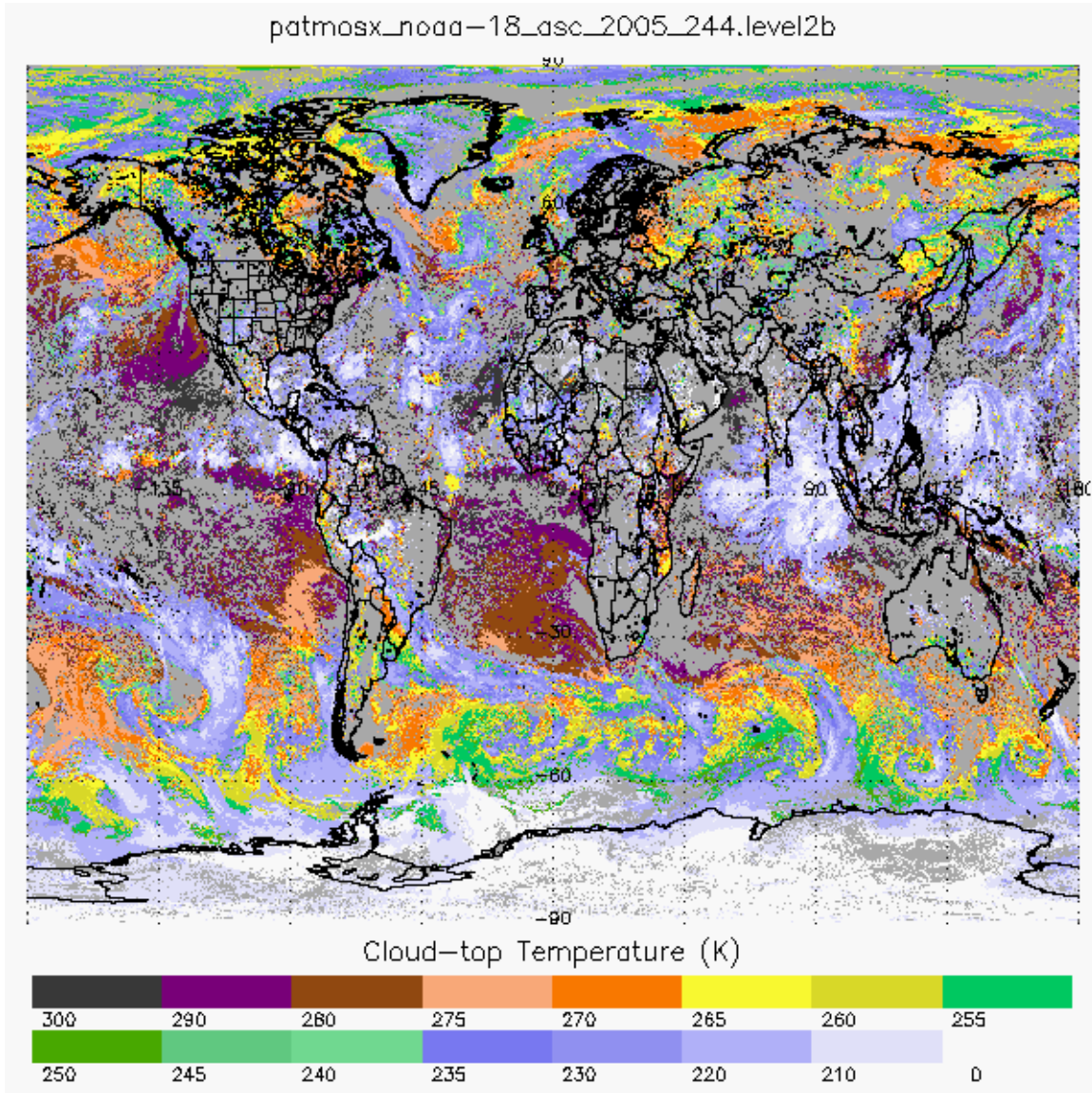
Figure 18: Example ACHA output of cloud-top temperature derived from NOAA-18 AVHRR data for September 1, 2005.
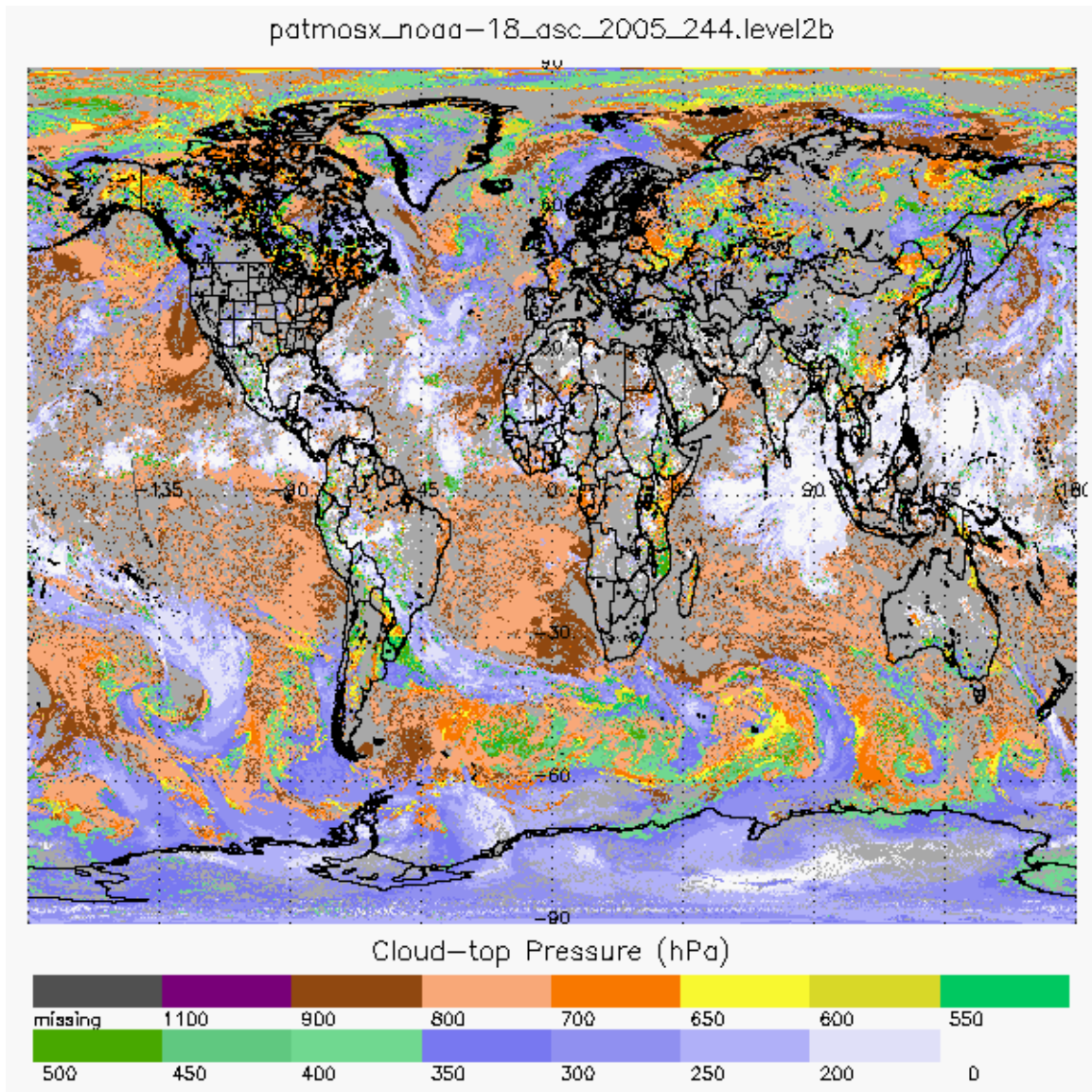
Figure 19: Example ACHA output of cloud-top pressure derived from NOAA-18 AVHRR data for September 1, 2005.
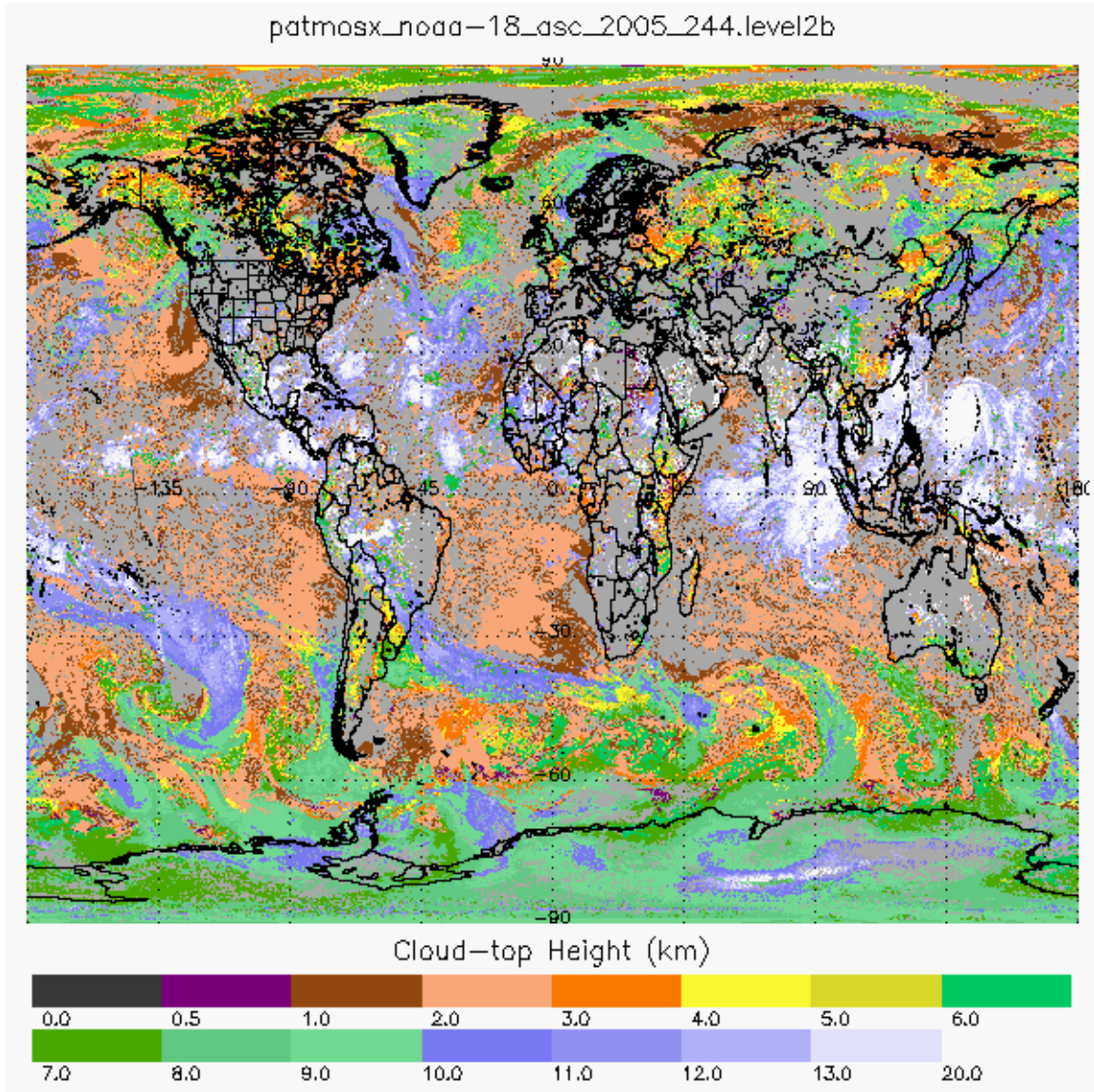
Figure 20: Example ACHA output of cloud-top height derived from NOAA-18
AVHRR data for September 1, 2005.

patmosx_noaa−18_asc_2005_244.level2b

cld_emiss_acha

0.00   0.20   0.40   0.60   0.80   1.00
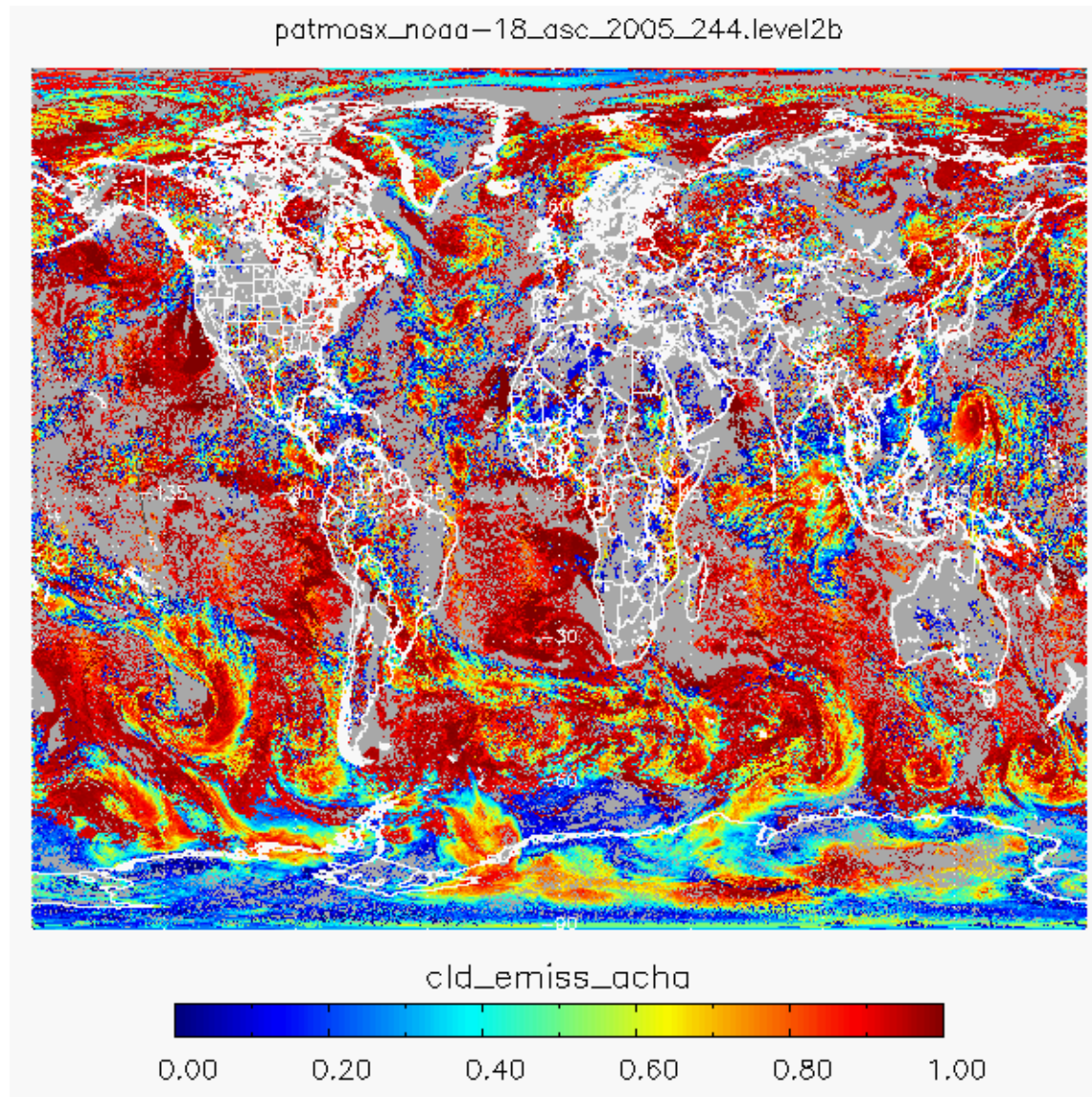
Figure 21: Example ACHA output of 11µm cloud emissivity derived from NOAA-18 AVHRR data for September 1, 2005.

4.2.2   Precision and Accuracy

To estimate the precision and accuracy of the ACHA, CALIPSO data from NASA EOS A-Train are used. This new data source provides unprecedented information on a global scale. While surface based sites provide similar information, the limited sampling they offer requires years of analysis to generate the amount of collocated data provided by CALIPSO in a short time period.

4.2.2.1   MODIS Analysis

The MODIS cloud height products (MYD06) have proven to be a useful and accurate source of information to the cloud remote sensing community. The MYD06 cloud height algorithm employs the longwave CO_2 channels in a CO_2 slicing approach to estimate the cloud-top pressure and cloud effective cloud amount. More details on this algorithm are available in the MODIS MYD06 ATBD (Menzel et al., 2006). The MODIS MYD06 ATBD quotes the cloud-top pressure accuracy to be roughly 50 mb, which is under the GOES-R ABI specification of 100 mb.

Given the wide use of the MYD06 product set, a comparison between the ACHA and MYD06 is warranted. While the MYD06 product set does provide the direct measure of cloud height provided by CALIPSO, it does complement the verification by providing qualitative comparisons over a larger domain. Given the availability of the longwave CO_2 channels on MODIS, we expect MYD06 to provide superior results especially for semitransparent cirrus.

To compare the ACHA results to those from MODIS, we analyzed Aqua MODIS data that were nearly coincident with SEVIRI observations. We currently use 3 MODIS granules that provide 15 minutes of data. We then compare these results to SEVIRI data that are closest in time. Our time threshold is 7.5 minutes. Both datasets are remapped to a constant projection with a spatial resolution of 0.08 degrees.

An example of this comparison is shown in **Figure 22**. In this figure, the top two panels show the MODIS and SEVIRI 0.65 μm reflectance images. The bottom left panel shows the time difference between the MODIS and SEVIRI data. The bottom right image shows the pixels used in this analysis. In addition to the time criteria, additional criteria for inclusion were placed on the agreement between the SEVIRI and MODIS observations.

In this analysis, only pixels where the 11 μm brightness temperatures agreed to within 4K and the 0.65 μm reflectance values agreed to with 5% were used. The rationale for these criteria is that agreement of cloud products is only expected for pixels, which have rough agreement in the observations. Any point that has a color (blue, green or red) is one that met the time and observation criteria. It is also assumed that cloud products should only agree when the cloud detection and phase results agree. The green points in **Figure 22** are those that met the additional criteria that both cloud masks were set to cloudy. The red pixels in **Figure 22** show the subset of points that also agreed on cloud phase. Note in **Figure 22** that while the filtering applied here dramatically reduces the number of points used in the analysis, the number of remaining points available for comparison still numbers over 5000 for this scene which, provides adequate sampling of relative performance of the ACHA algorithms compared to the MODIS algorithms.
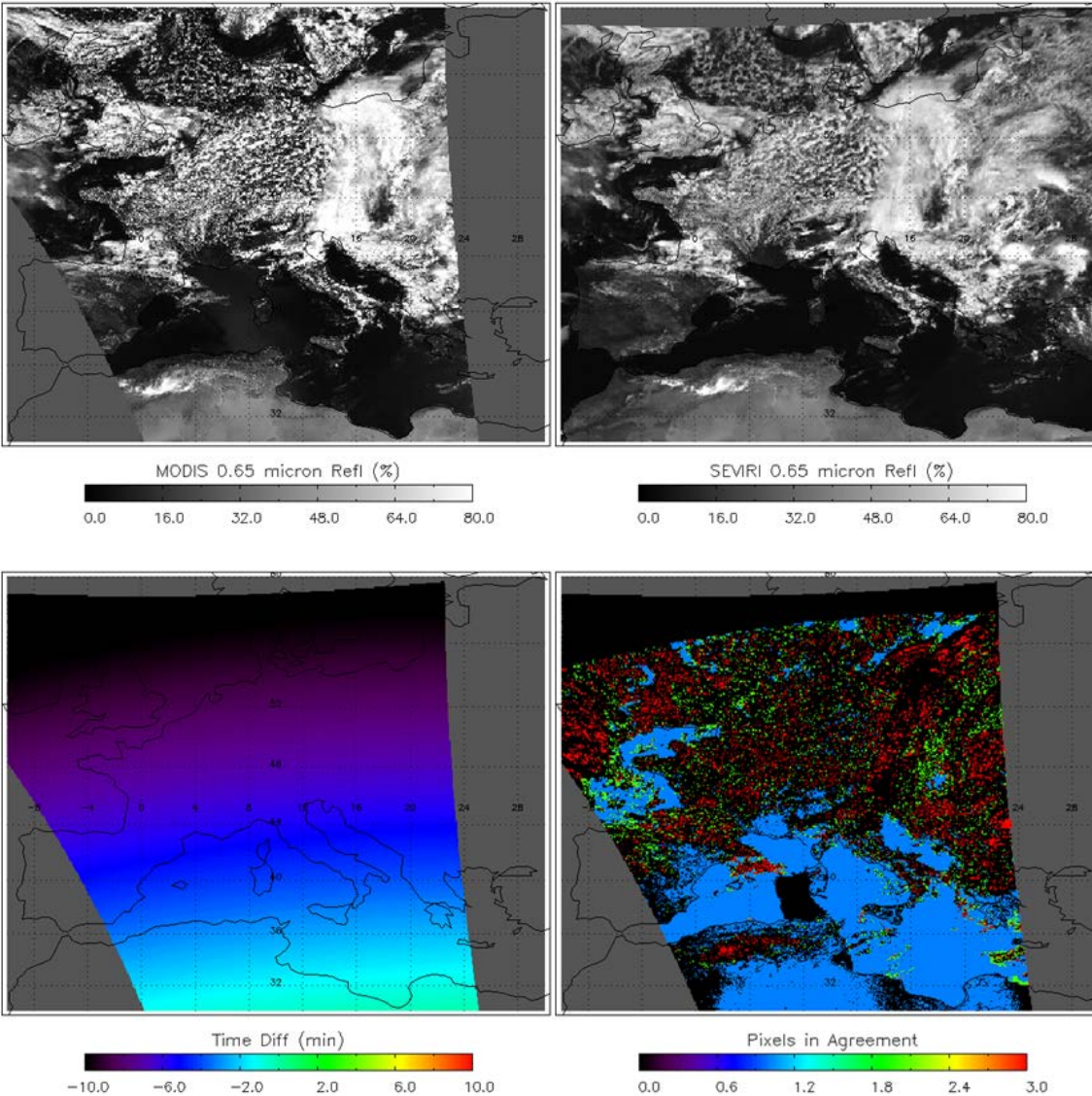
Figure 22: Example images illustrating a comparison of MODIS and SEVIRI data. Image at the top right shows the MODIS 0.65 μm reflectance. Top left image shows the SEVIRI 0.65 μm reflectance. Bottom left image shows the time difference in minutes. Bottom right image shows the pixels used in the analysis. Black colored regions were excluded based on differences in the MODIS and SEVIRI 0.65 μm reflectance and 11 μm brightness temperature. Red, green and blue colored pixels were used in the analysis.

4.2.2.1.1   Comparison of Cloud-top Pressure

Figure 23 shows a comparison of the cloud-top pressure results from those SEVIRI and MODIS points that met all of the criteria described above. No additional filtering on the cloud top pressure values was applied. The results indicate that the MYD06 cloud-top pressures were on average 23.48 hPa lower in the atmosphere than the ACHA

results with a standard deviation of 80 hPa. Although comparing two passive satellite measurements cannot be thought of as validation, the bias and precision estimates of the ACHA relative to MODIS indicate the AWG algorithm is performing well.
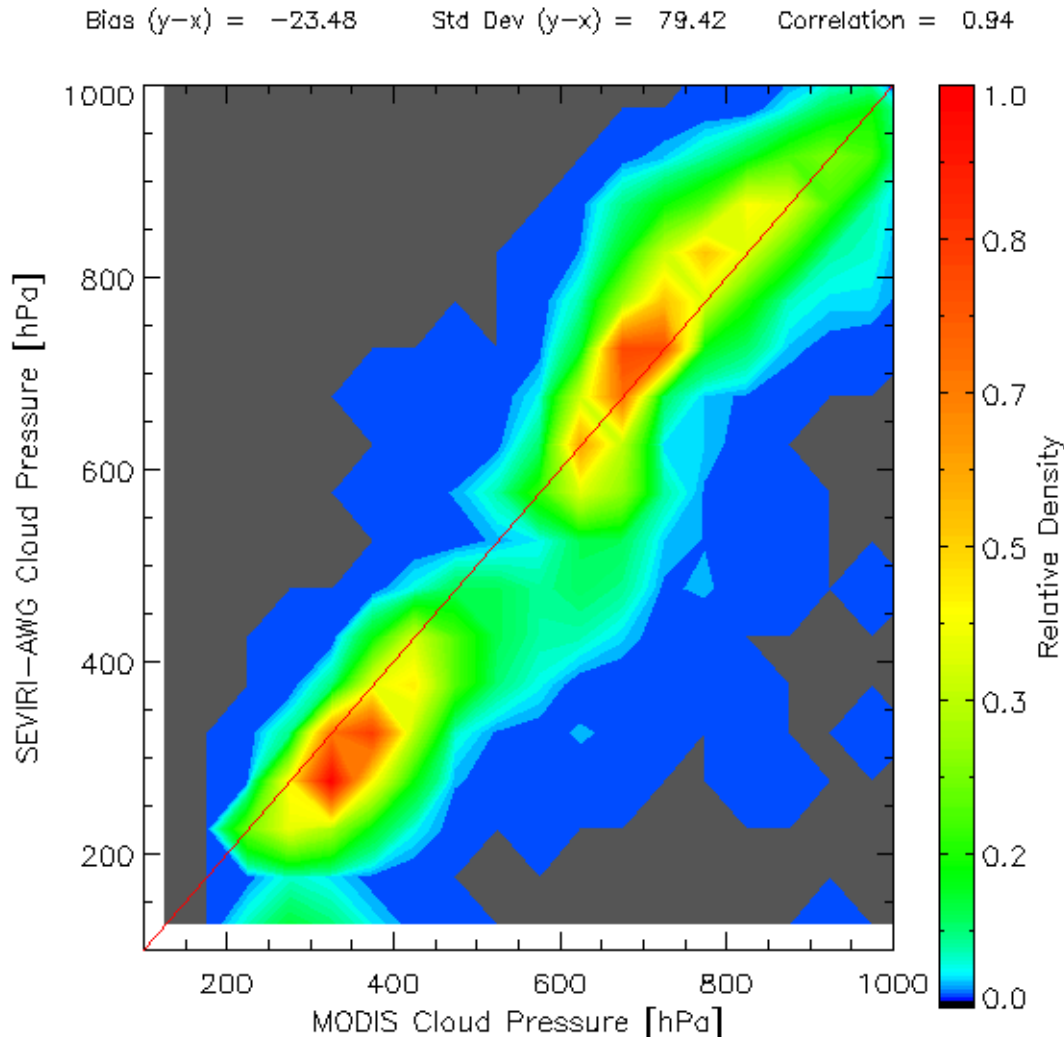
Figure 23: Comparison of cloud-top pressure for June 13, 2008 at 12:15 UTC over Western Europe derived from the MODIS (MYD06) products and from the Cloud Application Team's baseline approach applied to SEVIRI data. Bias (accuracy) and the standard deviation (precision) of the comparison are shown in the figure.

4.2.2.1.2   Comparison of Cloud-top Temperature

An analogous comparison to that shown in **Figure 23** constructed for cloud-top temperature is shown in **Figure 24**. As was the case for cloud-top pressure, the cloud-top

temperature comparison shows that the ACHA algorithm applied to SEVIRI is meeting specification relative to MODIS for this scene.
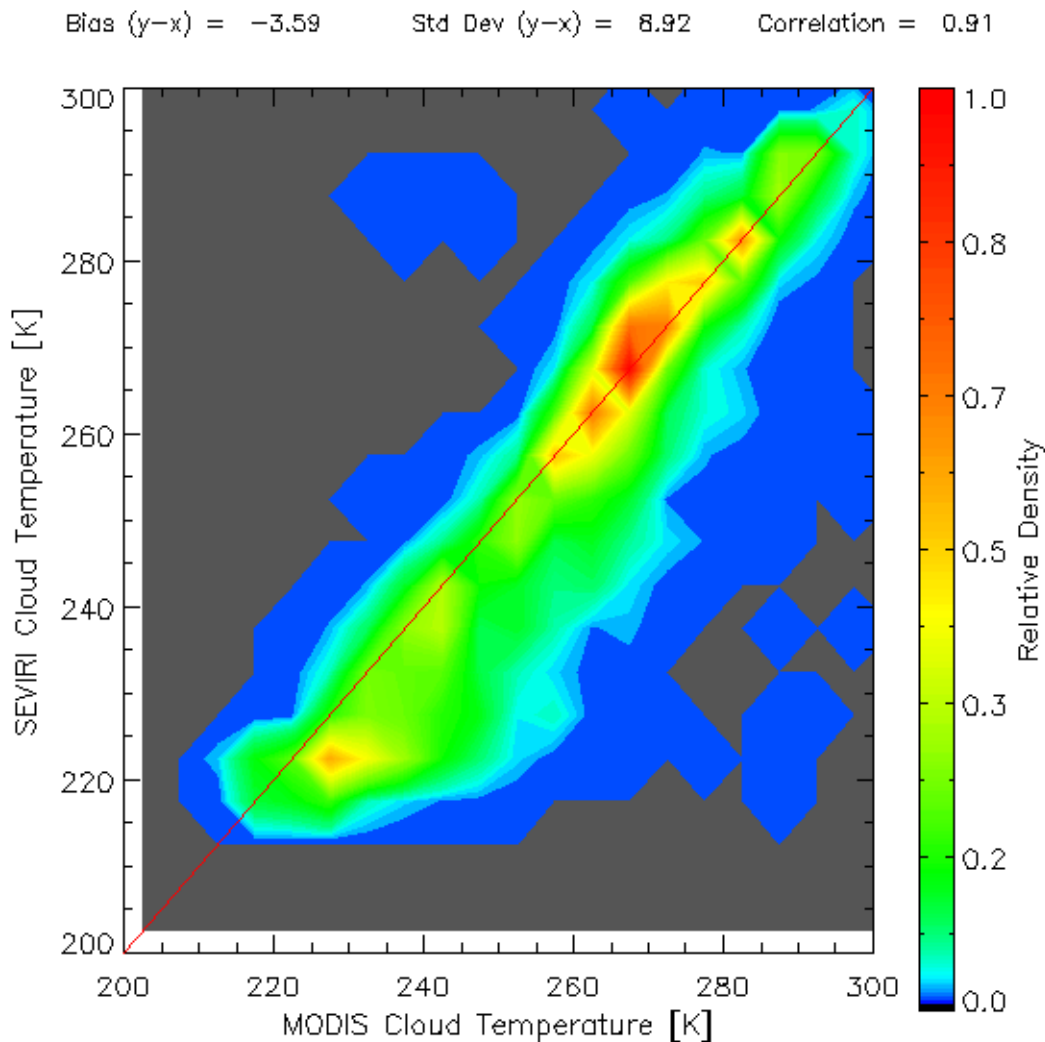
Figure 24: Comparison of cloud-top temperature for June 13, 2008 at 12:15 UTC over Western Europe derived from the MODIS (MYD06) products and from the Cloud Application Team's baseline approach applied to SEVIRI data. Bias (accuracy) and the standard deviation (precision) of the comparison are shown in the figure.

4.2.2.2 CALIPSO Analysis

The CALIPSO/CALIOP data (hereafter referred to as CALIPSO) provide unique information on the cloud vertical structure that can be used to validate the ACHA.

A controlled copy of this document is maintained in the CDR Program Library.
Approved for public release. Distribution is unlimited.

60

For this analysis, a collocation tool has been developed to determine the relevant information provided by CALIPSO for each collocated SEVIRI pixel. This tool has been applied to all SEVIRI data for the datasets specified in section 4.1. For each SEVIRI pixel that is collocated with CALIPSO data, the following information is available:

- Time difference between SEVIRI and CALIPSO,

- Number of cloud layers observed by CALIPSO,

- Cloud-top height of highest cloud layer, and

- Cloud-top temperature of highest cloud layer

In addition to the above information, the SEVIRI 11 μm radiances and the computed clear-sky radiances are used to estimate the cloud emissivity assuming the cloud existed at the height given by CALIPSO. The analysis done spanned data from August 2006 (summer), February 2007 (winter), April 2007 (spring) and October 2007 (fall) over the entire SEVIRI domain and encompassed the full range of conditions. The analysis shown in this section proves the performance of the ACHA based on the cloud height and cloud emissivity as derived from CALIPSO. The height bins were set to a width of 1 km thick and range from 0 to 20 km. The cloud emissivity bins were set to a width of 0.1 and range from -0.2 and 1.2. Emissivities less than 0 imply the observed radiance was less than the clear-sky radiance and emissivities greater than 1.0 imply that the observed radiance was greater than the blackbody emission at the CALIPSO cloud temperature. Only data that were called cloudy by the GOES-R AWG cloud mask (ACM) and by CALIPSO were included in this analysis. **Figure 25** shows the total number of pixels and their distribution in Z_c-e_c space for this analysis. Any cells that are colored grey did not have enough points for analysis.
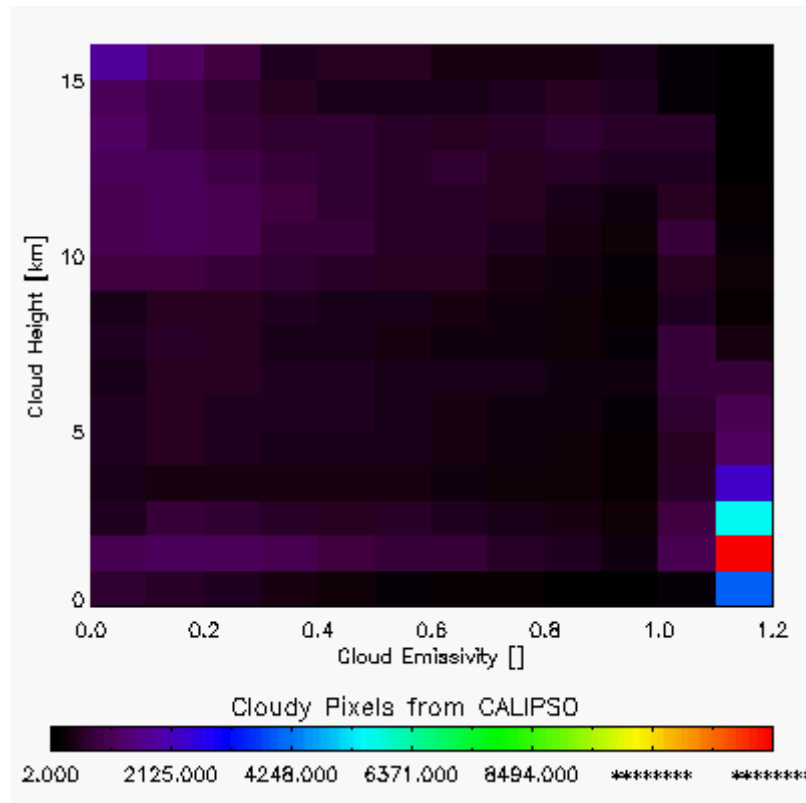
Figure 25: Distribution of points used in the validation of the ACHA applied to SEVIRI data for data observed during simultaneous SEVIRI and CALIPSO periods over eight weeks from four seasons in 2006 and 2007.

4.2.2.2.1 Validation of Cloud Top Height

For each Z_c – e_c bin, the bias in the ACHA – CALIPSO results was compiled. In addition, the standard deviation of the bias (ACHA – CALIPSO) in each bin was also computed. In terms of accuracy and precision, the mean bias is the accuracy and standard deviation of the bias is the precision. The resulting distributions of the mean of the bias and its standard deviation are shown in Figures 26-27. The F&PS specification for accuracy is 0.5 km for low-level clouds with $e_c > 0.5$. While the accuracy is well below this value for the stated cloudiness stratification, the precision of the bias approaches this number.

This analysis indicates that the precision in cloud height for low-level clouds with $e_c > 0.5$ is dominated by the handling of low-level temperature inversions. This situation is a problem for all infrared methods and coordination with the GOES-R Winds Team is in progress to optimize our performance for these clouds. The other area of concern is the standard deviation of the bias for optically thin cirrus. Work is being done to improve in this area as well and involves incorporating radiance biases to improve our ability to reproduce the cirrus observations and use of the water vapor channels to increase the sensitivity to cloud height for these clouds.
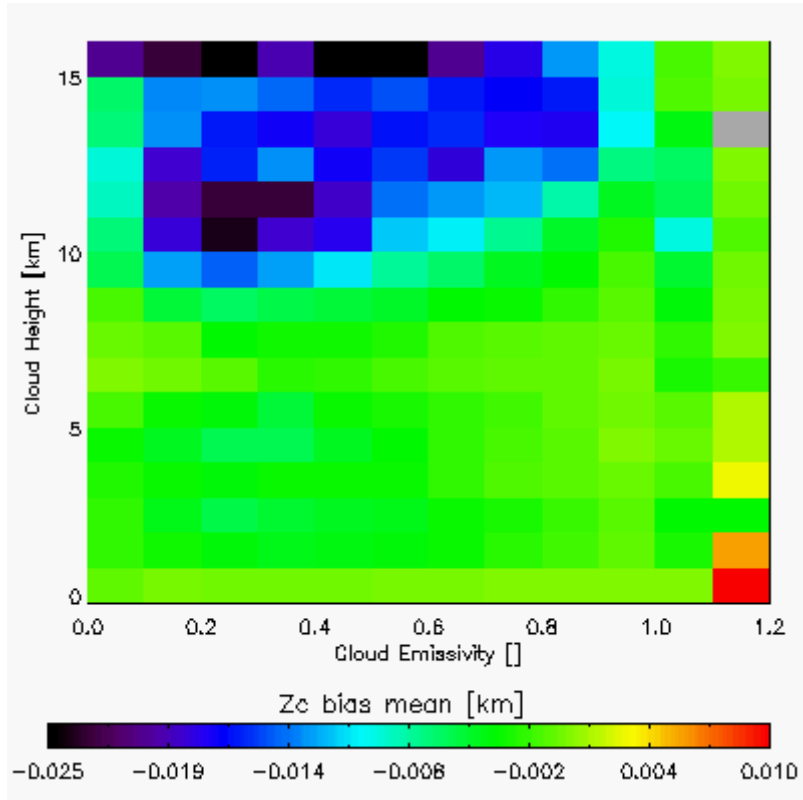
Figure 26: Distribution of cloud-top height mean bias (accuracy) as a function of cloud height and cloud emissivity as derived from CALIPSO data for all SEVIRI observations for four two-week periods covering all seasons. Bias is defined as ACHA – CALIPSO.
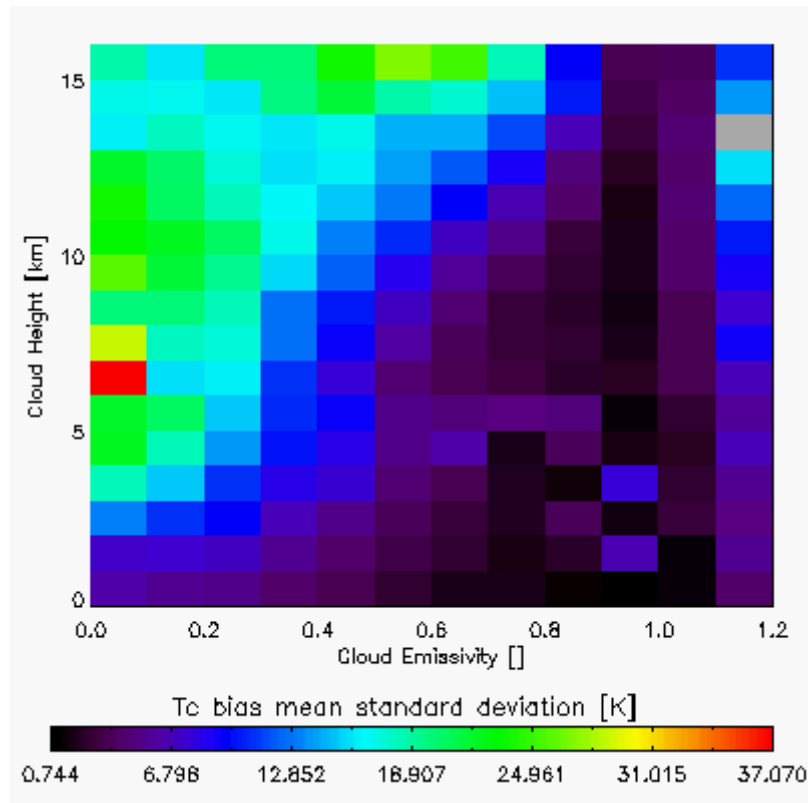
Figure 27: Distribution of cloud-top height of the standard deviation of the bias (precision) as a function of cloud height and cloud emissivity as derived from CALIPSO data for all SEVIRI for four two-week periods covering all seasons. Bias is defined as ACHA – CALIPSO.

4.2.2.2.2   Validation of Cloud Top Temperature

The same analysis was applied to the verification of cloud-top temperature. The resulting mean (accuracy) and standard deviation (precision) of the bias results are shown in Figures 28-29. As expected, the T_c results show the same pattern as the Z_c results. As was the case with the cloud height analysis above, the accuracy of the cloud temperature is very good and meets the F&PS accuracy requirement. As with cloud height, the precision of the cloud temperature results relative to CALIPSO is much worse than the accuracy. The F&PS specification for accuracy for cloud-top temperature is 1 K for purely black-body cloud in a known atmosphere. None of the observed clouds ever meet these restrictions, and therefore the verification of the cloud-top temperature F&PS specification is impossible with real data or realistic simulations.

A controlled copy of this document is maintained in the CDR Program Library.
Approved for public release. Distribution is unlimited.

64
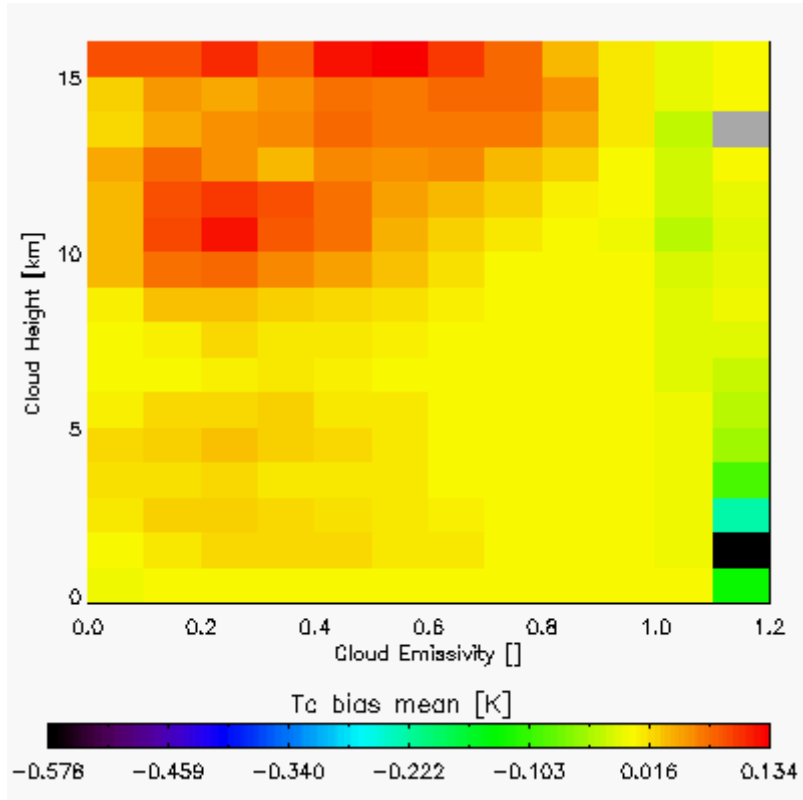
Figure 28: Distribution of cloud-top temperature mean bias (accuracy as a function of cloud height and cloud emissivity as derived from CALIPSO data for all SEVIRI observations for four two-week periods covering all seasons. Bias is defined as ACHA – CALIPSO.
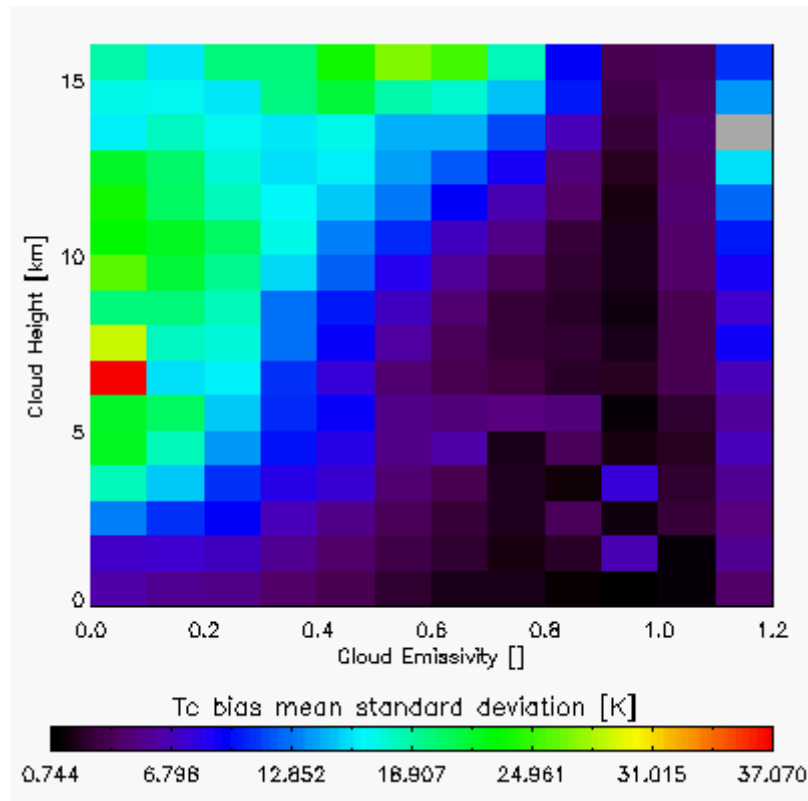
Figure 29: Distribution of cloud-top temperature of the standard deviation of the bias (precision) as a function of cloud height and cloud emissivity as derived from CALIPSO data for all SEVIRI observations for four two-week periods covering all seasons. Bias is defined as ACHA – CALIPSO.

4.2.2.2.3 Validation of Cloud Top Pressure

The current suite of CALIPSO products does not include pressure as a product. We are modifying our tools to estimate cloud pressure from the cloud height products in the CALIPSO product suite. However, the cloud-top pressure errors are highly correlated to the cloud-top height errors shown above. The comparisons to MODIS confirm this correlation.

4.2.3   Error Budget

Using the validation described above, the following table provides our preliminary estimate of an error budget. The "Bias Estimate" column values most closely match our interpretation of the F&PS accuracy specifications. To match the F&PS, these numbers were generated for low-level clouds with emissivities greater than 0.8. Cloud pressure errors were estimated assuming 1000m = 100 hPa which is a good approximation at low levels.

Table 27: Preliminary estimate of error budget for ACHA.

Product	Accuracy Specification (F&PS)	Bias Estimate	Precision Specification (F&PS)	Standard Deviation Estimate
Cloud-top Temperature	4 K	-0.22 K	5 K	4.75 K
Cloud-top Height	0.5 km	-0.0002 km	1.5 km	0.94 km
Cloud-top Pressure	100 hPa	-0.02 hPa	150 hPa	94 hPa

As **Table 27** shows, the ACHA meets the 100% F&PS requirements for precision and accuracy. It is important to identify the three main drivers of the ACHA error budget.

- *Lack of Knowledge of Low-level Inversions.* The current F&PS specifications demand accurate performance of cloud height for low-level clouds. Even if the instrument and retrievals are perfect and an accurate cloud-top temperature is estimated, the unknown effects of inversions can result in cloud heights failing to meet specification.

- *Characterization of Channel 16.* Our ability to place cirrus properly is in large part determined by our ability to model the observations within absorption bands (ch16). If poor instrument characterization or manufacture results in unknown spectral response functions, the ability to perform well in the presence of cirrus clouds is in jeopardy.

- *Multi-layer clouds.* While the AWG cloud type algorithm does include a multi-layer detection, our knowledge of the properties of that lower cloud is limited.

The Cloud Application Team will continue to be involved in developments that impact the above error sources.

A controlled copy of this document is maintained in the CDR Program Library.

Approved for public release. Distribution is unlimited.

67

5.   Practical Considerations

5.1   Numerical Computation Considerations

The ACHA employs an optimal estimation approach. Therefore, it requires inversions of matrices that can, under severe scenarios, become ill-conditioned. Currently, these events are detected and treated as failed retrievals.

5.2   Programming and Procedural Considerations

The ACHA makes heavy use of clear-sky RTM calculations. The current system computes the clear-sky RTM at low spatial resolution and with enough angular resolution to capture sub-grid variation to path-length changes. This approach is important for latency consideration as the latency requirements could not be met if the clear-sky RTM were computed for each pixel.

5.3   Quality Assessment and Diagnostics

The optimal estimation framework provides automatic diagnostic metrics and estimates of the retrieval error. It is recommended that the optimal estimation covariance matrices be visualized and analyzed on a regular basis. In addition, the CALIPSO analysis described above should be done regularly.

5.4   Exception Handling

The ACHA includes checking the validity of each channel before applying the appropriate test. The ACHA also expects the processing framework to flag any pixels with missing geolocation or viewing geometry information.

The ACHA does check for conditions where the ACHA cannot be performed. These conditions include saturated channels or missing RTM values. In these cases, the appropriate flag is set to indicate that no cloud temperature, pressure and height are produced for that pixel. In addition, a fill value is stored for the cloud temperature, pressure and height at these pixels.

5.5   Algorithm Validation

It is recommended that the CALIPSO analysis described earlier be adopted as the main validation tool. If CALIPSO type observations are not available, use of surface-based lidars and radars, such as provided by the Atmospheric Radiation Measurement (ARM) program, is recommended.

5.6   Processing Environment and Resources

Processing and data generation resources used are located at The University of Wisconsin – Madison, Space Science and Engineering Center (SSEC). Those resources

include a Linux-based share science computing cluster using ~50 concurrent processors with a multi-node storage array containing sufficient space to store the PATMOS-x TCDR and FCDR as well as the precursor AVHRR Level1b and ancillary data products. Total space required is ~30TB. With the current hardware configuration we estimate we can process the entire AVHRR record and generate the PATMOS-x product in three weeks.

6.   Assumptions and Limitations

The following sections describe the current limitations and assumptions in the current version of the ACHA.

6.1   Algorithm Performance

Assumptions have been made in developing and estimating the performance of the ACHA. The following list contains the current assumptions and proposed mitigation strategies.

1. NWP data of comparable or superior quality to the current 6 hourly GFS forecasts are available.   (Use longer range GFS forecasts or switch to another NWP source – ECMWF.)

2. RTM calculations are available for each pixel. (Use reduced vertical or spatial resolution in driving the RTM.)

3. All of the static ancillary data are available at the pixel level. (Reduce the spatial resolution of the surface type, land/sea mask and or coast mask.)

4. The processing system allows for processing of multiple pixels at once for use of spatial texture information. (No mitigation possible)

For a given pixel, should any channel not be available, the ACHA algorithm will not be performed on that particular pixel.

6.2   Sensor Performance

It is assumed that the satellite sensor will meet its current specifications. However, the ACHA will be dependent on the following instrument characteristic:

- Unknown spectral shifts in some channels will cause biases in the clear-sky RTM calculations that may impact the performance of the ACHA.

7.   Future Enhancements

While development of the baseline ACHA continues, we expect in the coming years to focus on the issues noted below.

7.1   Optimization for Derived Motion Winds

The DMW team is critically dependent on the performance of this algorithm. In addition, the DMW team has a long heritage of making its own internal estimates of cloud-top height. Therefore, it is important that the CAT and DMW teams work together, particularly on the issue of atmospheric inversions.

7.2   Implementation of Channel Bias Corrections

The MYD06 development team has found that bias corrections are critical for the proper use of infrared channels for cloud height estimation. Currently, we utilize no bias corrections in ACHA.   In addition, we plan to implement a mechanism to account for the large surface biases in NWP data.

7.3   Use of 10.4 μm Channel

The 10.4 $\Box$m channel is new incorporate this channel into the ACHA to improve our cloud microphysical retrievals. We expect the GOES-R Risk Reduction projects to demonstrate its use before implementation into the operational algorithm.

A controlled copy of this document is maintained in the CDR Program Library.
Approved for public release. Distribution is unlimited.

71

8.   References

GOES-R ABI Algorithm Interface and Ancillary Data Description Document.

GOES-R ABI Cloud Mask Algorithm Theoretical Basis Document.

GOES-R ABI Cloud Type/Phase Algorithm Theoretical Basis Document.

GOES-R Acronym and Glossary (P417-R-LIST-0142).

GOES-R Level 1 Requirements Document (L1RD).

GOES-R Series Ground Segment (GS) Project Functional and Performance Specification (F&PS) [G417-R-FPS-0089].

GOES-R Series Mission Requirements Document (MRD) [P417-R-MRD-0070].

Hannon, S., Strow, L.L. and Mcmillan, W.W., (1996). Atmospheric infrared fast transmittance models: a comparison of two approaches. *Optical Spectroscopic Techniques and Instrumentation for Atmospheric and Space Research II Proc. SPIE,* 2830:94-105.

Hansen, M., R. DeFries, J.R.G. Townshend, and Sohlberg, R., (1998). UMD Global Land Cover Classification, 1 Kilometer, 1.0, Department of Geography, University of Maryland, College Park, Maryland, 1981-1994.

Heidinger, Andrew K.; Evan, Amato T.; Foster, Michael J. and Walther, Andi., (2012). A naive Bayesian cloud-detection scheme derived from CALIPSO and applied within PATMOS-x. *Journal of Applied Meteorology and Climatology*, Volume 51:Issue 6:1129-1144.

Heidinger, A. K.; Pavolonis, M. J.; Holz, R. E.; Baum, Bryan A. and Berthier, S., (2010). Using CALIPSO to explore the sensitivity to cirrus height in the infrared observations from NPOESS/VIIRS and GOES-R/ABI. *Journal of Geophysical Research*, Volume 115:Doi:10.1029/2009JD012152.

Heidinger, Andrew K. and Pavolonis, Michael J., (2009). Gazing at cirrus clouds for 25 years through a split window, part 1: Methodology. *Journal of Applied Meteorology and Climatology*, Volume 48:Issue 6:1100-1116.

Menzel, W.P., Frey, R.A., Baum, B.A., and Zhang H., (2006). Cloud Top Properties and Cloud Phase - Algorithm Theoretical Basis Document. Products: 06-L2, 08-D3, 08-E3, 08-M3. NASA Goddard Space Flight Center, Tech. Rep. ATBD Reference Number: ATBD-MOD-05.

Rodgers, C.D., (1976). Retrieval of atmospheric temperature and composition from remote measurements of thermal radiation. *Rev. Geophys. Space Phys*., 60:609-624.

Seemann, S.W., Borbas, E.E, Knuteson, R.O., Stephenson, G.R., Huang, H.-L., (2008). Development of a global infrared land surface emissivity database for application to clear sky sounding retrievals from multi-spectral satellite radiance measurements*. Journal of Applied Meteorology and Climatology*, Volume 47:Issue 1:108-123.

Yang, P., Wei, H., Huang, H.-L., Baum, B.A., Hu, Y.X., Kattawar, G.W., Mishchenko, M.I., and Fu, Q., (2005). Scattering and absorption property database for nonspherical ice particles in the near-through far-infrared spectral region. *Appl. Opt.,* 44:5512–5523.

Appendix A.   Acronyms and Abbreviations

Acronym or Abbreviation	Meaning
1DVAR	One Dimensional Variational
ABI	Advanced Baseline Imager
ACHA	GOES-R ABI Cloud Height Algorithm
AIT	Algorithm Integration Team
AMV	Atmospheric Motion Vectors
A-Train	Afternoon Train (Aqua, CALIPSO, CloudSat, etc.)
AVHRR	Advanced Very High Resolution Radiometer
AWG	Algorithm Working Group
BT	Brightness Temperature
BTD	Brightness Temperature Difference
C-ATBD	Climate Algorithm Theoretical Basis Document
CALIPSO	Cloud-Aerosol Lidar and Infrared Pathfinder Satellite
CDR	Climate Data Record
CFSR	Climate Forecast System Reanalysis
CIMSS	Cooperative Institute for Meteorological Satellite Studies
CLAVR-x	Clouds from the AVHRR Extended
CRTM	Community Radiative Transfer Model
DMW	Derived Motion Winds
ECMWF	European Centre for Medium-Range Weather Forecasts
EOS	Earth Observing System
EUMETSAT	European Organization for the Exploitation of Meteorological Satellites
F&PS	Function and Performance Specification
GAC	Global Area Coverage
GFS	Global Forecast System
GOES	Geostationary Operational Environmental Satellite
GOES-RRR	GOES-R Risk Reduction
IR	Infrared
IRW	IR Window
ISCCP	International Satellite Cloud Climatology Project
LUTS	Look up tables

MODIS	Moderate Resolution Imaging Spectroradiometer
MSG	Meteosat Second Generation
NASA	National Aeronautics and Space Administration
NCDC	National Climatic Data Center
NESDIS	National Environmental Satellite, Data, and Information Service
NOAA	National Oceanic and Atmospheric Administration
NWP	Numerical Weather Prediction
PATMOS-x	AVHRR Pathfinder Atmospheres – Extended
PFAAST	Pressure layer Fast Algorithm for Atmospheric Transmittances
PLOD	Pressure Layer Optical Depth
RTM	Radiative Transfer Model
SEVIRI	Spinning Enhanced Visible and Infrared Imager
SSEC	Space Science and Engineering Center
STAR	Center for Satellite Applications and Research
VIIRS	Visible Infrared Imager Radiometer Suite
UW	University of Wisconsin at Madison

Appendix B.   Dataset Variables

This table lists the data and coordinate variables included in the level2 data files along with their data types, dimensions, and descriptions.

Variable Name	Data Type	Dimensions	Description
acha_info	byte	time,latitude,longitude	processing information for ACHA (0=no/1=yes) 1:Cloud Height Attempted 2:Bias Correction Employed 3:Ice Cloud Retrieval 4:Local Radiative Center Processing Used 5:Multi-layer Retrieval 6:Lower Cloud Interpolation Used 7:Boundary Layer Inversion Assumed
acha_quality	byte	time,latitude,longitude	quality flags for ACHA products 1:Processed (0=no,1=yes) 2:valid Tc retrieval (1=yes,0=no) 3:valid ec retrieval (1=yes,0=no) 4:valid beta retrieval (1=yes,0=no) 5:degraded Tc retrieval (1=yes,0=no) 6:degraded ec retrieval (1=yes,0=no) 7:degraded beta retrieval (1=yes,0=no)
bad_pixel_mask	byte	time,latitude,longitude	mask that distinguishes good(0) from bad(1) pixels
cld_emiss_acha	byte	time,latitude,longitude	cloud emissivity at the nominal wavelength of 11 microns, determined from the AWG cloud height algorithm - NOAA CDR
cld_height_acha	short	time,latitude,longitude	cloud height computed using the AWG cloud height algorithm
cld_height_uncer_acha	byte	time,latitude,longitude	cloud height uncertainty computed using the AWG cloud height algorithm
cld_opd_dcomp	short	time,latitude,longitude	cloud optical depth at the nominal wavelength of 0.65 microns, determined from DCOMP - NOAA CDR
cld_opd_dcomp_unc	short	time,latitude,longitude	uncertainty in the log10 cloud optical depth at the nominal wavelength of 0.65 microns, determined from DCOMP; see attributes for channels used
cld_press_acha	short	time,latitude,longitude	cloud-top pressure computed using the AWG cloud height algorithm

cld_reff_acha	byte	time,latitude,longitude	effective radius of cloud particles determined from ACHA; see attributes for channels used
cld_reff_dcomp	short	time,latitude,longitude	effective radius of cloud particles determined from DCOMP; see attributes for channels used - NOAA CDR
cld_reff_dcomp_unc	short	time,latitude,longitude	uncertainty in the log10 effective radius of cloud particle determined from DCOMP; see attributes for channels used
cld_temp_acha	short	time,latitude,longitude	cloud-top temperature computed using the AWG cloud height algorithm - NOAA CDR
cloud_fraction	byte	time,latitude,longitude	cloud fraction computed over a 3x3 pixel array at the native resolution centered on this pixel
cloud_fraction_uncertainty	byte	time,latitude,longitude	cloud fraction uncertainty computed over a 3x3 array
cloud_mask	byte	time,latitude,longitude	integer classification of the cloud mask including clear=0, probably-clear=1, probably-cloudy=2, cloudy=3
cloud_probability	byte	time,latitude,longitude	probability of a pixel being cloudy from the Bayesian cloud mask
cloud_transmission_0_65um_nom	byte	time,latitude,longitude	cloud transmission 0.65 microns nominal from DCOMP
cloud_type	byte	time,latitude,longitude	integer classification of the cloud type including clear and aerosol type,0=clear,1=probably clear,2=fog,3=water,4=supercooled water,5=mixed,6=opaque_ice,7=cirrus,8=overlapping,9=overshooting,10=unknown,11=dust,12=smoke
cloud_water_path	byte	time,latitude,longitude	integrated total cloud water over whole column
dcomp_info	short	time,latitude,longitude	processing flags for DCOMP 1:info flag set ? (0=no,1=yes) 2:land/sea mask (0=land,1=sea) 3:day/night mask (0=Day,1=Night) 4:twilight (65-82 solar zenith) (0=no,1=yes) 5:snow (0=no,1= snow) 6:sea-ice (0=no,1=sea-ice) 7:phase (0=liquid,1=ice) 8:thick_cloud (0=no,1=yes) 9:thin_cloud (0=no,1=yes)

A controlled copy of this document is maintained in the CDR Program Library.

Approved for public release. Distribution is unlimited.

77

dcomp_quality	byte	time,latitude,longitude	quality flags for DCOMP products 1:Processed (0=no,1=yes) 2:valid COD retrieval (0=yes,1=no) 3:valid REF retrieval (0=yes,1=no) 4:degraded COD retrieval (0=no,1=degraded) 5:degraded REF retrieval (0=no,1=degraded) 6:convergency (0=no,1=yes) 7:glint (0=no,1=yes)
glint_mask	byte	time,latitude,longitude	glint mask (0=no) (1=yes)
land_class	byte	time,latitude,longitude	land classes and values:shallow ocean=0,land=1,coastline=2,shallow inland water=3,ephemeral water=4,deep inland water=5,moderate ocean=6,deep ocean=7
latitude	float	latitude	latitude
longitude	float	longitude	longitude
refl_0_65um_nom	short	time,latitude,longitude	top of atmosphere reflectance at the nominal wavelength of 0.65 microns - NOAA CDR
refl_0_65um_nom_counts	short	time,latitude,longitude	instrument counts for the nominal 0.65 micron channel
refl_0_65um_nom_stddev_3x3	byte	time,latitude,longitude	standard deviation of the 0.63 micron reflectance computed over a 3x3 pixel array
refl_0_86um_nom	short	time,latitude,longitude	top of atmosphere reflectance at the nominal wavelength of 0.86 microns - NOAA CDR
refl_0_86um_nom_counts	short	time,latitude,longitude	instrument counts for the nominal 0.86 micron channel
refl_1_60um_nom	short	time,latitude,longitude	top of atmosphere reflectance at the nominal wavelength of 1.60 microns - NOAA CDR
refl_1_60um_nom_counts	short	time,latitude,longitude	instrument counts for the nominal 1.6 micron channel
refl_3_75um_nom	short	time,latitude,longitude	top of atmosphere reflectance at the nominal wavelength of 3.75 microns - NOAA CDR
relative_azimuth_angle	byte	time,latitude,longitude	relative azimuth angle in degrees. 0 is the principal plane looking towards sun
scan_element_number	int	time,latitude,longitude	scan element index of the pixel chosen for inclusion in level-2b
scan_line_number	int	time,latitude,longitude	scan line number

scan_line_time	float	time,latitude,longitude	time for the scan line in fractional hours
sensor_zenith_angle	byte	time,latitude,longitude	sensor zenith for each pixel measured in degrees from nadir
snow_class	byte	time,latitude,longitude	snow classes and values:no snow/ice=1,sea_ice=2,snow=3
solar_azimuth_angle	byte	time,latitude,longitude	solar azimuth angle in degrees from north, pixel to sun, positive values are clockwise from north
solar_zenith_angle	byte	time,latitude,longitude	solar zenith for each pixel measured in degrees away from the sun (0=looking at sun)
surface_temperature_retrieved	byte	time,latitude,longitude	surface temperature retrieved using atmospherically corrected 11 micron radiance
surface_type	byte	time,latitude,longitude	UMD surface type: water=0,evergreen_needle=1,evergreen_broad=2,deciduous_needle=3,deciduous_broad=4,mixed_forest=5,woodlands=6,wooded_grass=7closed_shrubs=8,open_shrubs=9,grasses=10,croplands=11,bare=12,urban=13
temp_11_0um_nom	short	time,latitude,longitude	top of atmosphere brightness temperature at the nominal wavelength of 11.0 microns - NOAA CDR
temp_11_0um_nom_clear_sky	short	time,latitude,longitude	top of atmosphere brightness temperature modeled assuming clear skies at the nominal wavelength of 11.0 microns
temp_11_0um_nom_stddev_3x3	byte	time,latitude,longitude	standard deviation of the 11 micron brightness temperature computed over a 3x3 pixel array
temp_12_0um_nom	short	time,latitude,longitude	top of atmosphere brightness temperature at the nominal wavelength of 12.0 microns - NOAA CDR
temp_3_75um_nom	short	time,latitude,longitude	top of atmosphere brightness temperature at the nominal wavelength of 3.75 microns - NOAA CDR
time	float	time,latitude,longitude	seconds since 1970-01-01 00:00:00